

Hot Nuclei - Landau Theory, Thermal Fluctuations and Dissipation*

Y. Alhassid

Center for Theoretical Physics, Sloane Physics Laboratory,
and A.W. Wright Nuclear Structure Laboratory,
Yale University, New Haven, Connecticut 06511

CONF-9010306--2

DE92 015008

Abstract. The basic ideas and theoretical methods used in the description of hot nuclei are reviewed. In particular, a macroscopic approach to shape transitions is discussed in the framework of the Landau theory in which the quadrupole shape degrees of freedom play the role of the order parameters. This theory describes the universal features of the nuclear shape evolution with temperature and spin. A unified description of fluctuations in all five quadrupole degrees of freedom is introduced and plays an important role in the calculation of physical observables. A macroscopic approach to the giant dipole resonance (GDR) in hot nuclei is developed. With all parameters fixed by the zero temperature nuclear properties, the theory predicts both the GDR cross-section and angular anisotropy of the γ -rays in very good agreement with recent experiments. The intrinsic shape fluctuations are the main cause for the resonance broadening at higher temperatures, while the orientation fluctuations are responsible for the observed attenuation in the angular anisotropy. Dissipation at finite temperature is discussed in the framework of a Langevin-like equation describing the time-dependent shape fluctuations. Non-adiabatic effects may cause motional narrowing of the resonance.

1. Introduction

The possibility of "heating up" a nucleus to a finite temperature opens for us a new dimension in the study of nuclear structure. The principal experimental techniques of forming such hot nuclei are via heavy ion fusion reactions with heavy projectiles. The relative kinetic energy in these collisions is deposited in internal excitations of the nucleus. If there is enough time this energy will be redistributed among the large number of degrees of freedom of the heavy compound nucleus and would lead to an equilibrated hot nucleus [1-3]. A typical heavy nucleus can store up to several hundred MeV of excitation energy in its dense "reservoir" of excited states.

Numerous phenomena are encountered in the study of hot nuclei [4-12]. Various phase-transition-like phenomena are expected to occur as we heat the nucleus. At critical temperatures of $T_c \sim 0.5-1$ MeV there is the disappearance of pairing [4], at $T_c \sim 1-3$ MeV we have the shape transitions of well deformed nuclei associated with the melting of the shell structure [5-7], and at $T_c \sim 7-12$ MeV there is the liquid-gas phase transition [8] above which the finite nucleus does not exist as such. The latter transition is hard to observe since Coulomb instabilities [8] start to develop at lower temperatures ($T \sim 5$ MeV). Of great interest both

* Invited talk presented at the Fifth Yukawa Memorial Symposium, Japan, October 25-26, 1990.

MASTER

FG02-91ER40608

experimentally [9-14] and theoretically [15-17] is the study of collective nuclear motion at finite temperature. In the following review we shall study mainly the shape transitions, the evolution of the nuclear shape with temperature and spin, and the collective nuclear motion at the corresponding range of temperatures and spins. However many of the theoretical techniques developed and discussed are useful in the description of other phenomena in hot nuclei.

The main theoretical methods used to describe hot nuclei are taken from statistical mechanics. However, since the nuclear system is finite (typically on the order of 100 degrees of freedom) these techniques should be applied with care. In particular we shall see that thermal fluctuations play a major role even away from the critical point.

Recent advances in detector systems are making it possible to study experimentally the properties of nuclei under conditions of high excitation and high spin. These properties are inferred from the measured spectra of γ -rays as well as of particles of low to medium mass that are emitted from the nuclear complex during its cooling process. A major probe of the shape of such hot nuclei is the giant dipole resonance [18-24] whose frequencies are known to depend on the nuclear shape.

The present review is organized as follows: In Section 2, we introduce the general concepts of hot nuclei: the equilibrium assumption and the definition of nuclear temperature and nuclear rotation. In Section 3, we discuss the various mean-field approximations used to treat hot rotating nuclei. The main discussion will focus on a recently developed macroscopic approach - the Landau theory of shape transitions [25,26]. Since the nuclear system is finite, fluctuations are important [27-32] and they will be introduced in Section 4, using the framework of the Landau theory. In Section 5, we shall introduce a macroscopic theory of the giant dipole resonance (GDR) in hot nuclei [29,32]. Comparison will be made to experimentally observed quantities - the GDR absorption cross-section and the angular anisotropy [33,34] of the GDR γ -rays observed in the decay of the hot nucleus. Dissipation at finite temperature is also an important issue. It is discussed in Section 6 in the context of time-dependent fluctuations [35,36]. If these fluctuations are non-adiabatic, they will lead to motional narrowing [37,38] in the GDR from which it is possible to determine certain friction coefficients. Section 7 discusses briefly the effect of fluctuations on the B(E2) transitions in the continuum which have been measured recently [39].

2. Hot Nuclei

2.1 The Equilibrium Assumption

At low energies the nuclear spectrum is discrete and a variety of theoretical models have been introduced to explain it. However, already for $E^* \geq 6$ MeV the level density of a heavy nucleus is so high that its spectrum is quasi-continuous. Individual states are then hard to resolve experimentally or theoretically. Some renouncement of knowledge is required in order for the problem to become tractable again. The basic underlying assumption is the equilibrium assumption: all states at a given excitation energy, spin and any other conserved quantum numbers are equally probable. It is only under this assumption that a reduced global

description of the nucleus in terms of a few macroscopic parameters can be achieved. The ensemble describing such a nucleus is the microcanonical ensemble.

Global equilibration means that various parts of the nucleus have enough time to reach complete relaxation and to explore all available phase space at the given excitation energy and spin. We shall refer to such a nucleus whose energy is shared among its many degrees of freedom as a hot nucleus. In a heavy ion reaction with a heavy projectile we expect that an important fraction of the fusion cross-section is the formation of an equilibrated nucleus. This is generally true for beam energy per nucleon of less than 5-7 MeV. It is of course an experimental task to identify that part of the cross-section which goes into the formation of an equilibrated hot nucleus [1-3].

2.2 Nuclear Temperature

The microcanonical ensemble at a given energy E which is proportional to $\delta(E-H)$ is not very convenient to work with. We therefore replace it by the canonical distribution $D \propto \exp(-H/T)$ at a certain temperature T . This temperature is determined by the condition that the average energy of the canonical ensemble is the given energy E . This leads to the following definition of nuclear temperature

$$\frac{1}{T} = \frac{d}{dE^*} \ln \rho(E^*) \quad (2.1)$$

where $\rho(E^*)$ is the nuclear level density at excitation energy E^* .

The formal relation [40] between the microcanonical and canonical ensembles is established when the canonical partition function

$$Z(T) = \text{Tr} e^{-H/T} \quad (2.2)$$

is evaluated in terms of the level density (which is the microcanonical partition function $\rho(E) = \text{Tr} \delta(E-H)$),

$$Z(T) = \int_0^{\infty} dE e^{-E/T} \rho(E) \quad (2.3)$$

The inverse relation to (2.3) is the inverse Laplace transform

$$\rho(E) = \frac{1}{2\pi i} \int_{-i\infty}^{i\infty} d\left(\frac{1}{T}\right) e^{E/T} Z(T) \quad (2.4)$$

If (2.4) is evaluated by the saddle point approximation we obtain the

relation (2.1). The exact transformation (2.4) represents the fluctuations in the inverse temperature for a fixed value of E.

2.3 Nuclear Rotation

In the formation of a compound nucleus in a heavy ion reaction the nucleus usually acquired large angular momentum. The microcanonical equilibrium ensemble is then proportional to $\delta(E-H)P_J$, where P_J is the projection on states with a given spin J. It is again convenient to transform to the temperature representation where we define a partition function at a given spin J to be

$$Z(T, J) = \text{Tr} (e^{-H/T} P_J) = \int_0^{\infty} dE e^{-E/T} \rho(E, J) \quad (2.5)$$

Here $\rho(E, J)$ is the level density at energy E and spin J. In terms of the density $\rho(E, M)$ with M being the spin projection [40]:

$$\rho(E, J) \approx - \frac{\partial}{\partial M} \rho(E, M) \Big|_{M=J+1/2} \quad (2.6)$$

Introducing the free energy in a frame rotating with angular velocity $\bar{\omega}$ [41]

$$F(T, \omega) = - T \ln \text{Tr} e^{- (H - \bar{\omega} \cdot \bar{J}) / T} \quad (2.7)$$

we can rewrite (2.5) in the form

$$Z(T, J) = \int_0^{4\pi T} \frac{i\omega d\omega}{4\pi T^2} e^{- [i(J+1/2)\omega + F(T, i\omega)] / T} \quad (2.8)$$

Thus by considering ω -fluctuations it is possible to calculate the partition function at a given spin. Usually (2.8) is evaluated at the saddle point approximation where ω is determined from J by the relation

$$J + 1/2 = - \partial F(T, \omega) / \partial \omega \quad (2.9)$$

This accomplishes the transformation from the description in terms of the extensive variables E and J to the intensive conjugate variables T and ω . The free energy in the rotating frame (2.7) is the fundamental relation which contains all the thermodynamic information on the system. In the next section we shall discuss how to calculate such a quantity.

3. Mean-Field and Landau Theories

Since H in (2.7) is a many-body Hamiltonian, the evaluation of the exact many-body partition function is difficult and approximation must be introduced. Most of them are based on various versions of the mean-field approximation.

3.1 Mean-Field Approximations

In general we seek to calculate the free energy $F=F(T,\omega;\rho)$ as a function of some trial parameters ρ . The equilibrium configuration is then found by minimizing F with respect to ρ .

The basic variational principle from which such approaches are derived is the following: The exact canonical density matrix $D=\exp(-H(T))/Z(T)$ is obtained by minimizing the free energy functional

$$F[T,D] = \text{Tr}(DH) + \text{Tr}(D \ln D) \quad (3.1)$$

with respect to all possible density matrices satisfying

$$\text{Tr} D = 1 \quad (3.2)$$

If we restrict the space of variations to density matrices of the form

$$D_0 \propto \exp(-H_0/T) \quad (3.3)$$

where H_0 is a one-body Hamiltonian, we find

$$F[T,\rho] = \text{tr} \left(t\rho + \frac{1}{2} \rho v \rho \right) + T \text{tr} \left[\rho \ln \rho + (1-\rho) \ln(1-\rho) \right] \quad (3.4)$$

Here ρ is the one-body density matrix and t and v are the one-body kinetic energy and two-body potential energy, respectively.

Minimizing F in (3.4) with respect to ρ , we obtained the finite-temperature Hartree-Fock equation [6]

$$\rho = \left(1 + \exp \left[\frac{(h_\rho - \mu)}{T} \right] \right)^{-1} \quad (3.5)$$

where

$$h_\rho = t + v\rho \quad (3.6)$$

is the mean-field single-particle Hamiltonian.

If we wish to include pairing effects we can do it within the finite-

temperature Hartree-Fock-Bogoliubov approximation [4].

If the phenomena we want to describe are the shape evolution with temperature and spin, a more restrictive choice of H_0 corresponds to that of the Nilsson Hamiltonian which is deformation-dependent but not self-consistent. The single-particle states with energies ϵ_i are assumed to be populated with the Fermi-Dirac occupation probabilities f_i

$$f_i = \frac{1}{1 + e^{(\epsilon_i - \mu)/T}} \quad (3.7)$$

To account for the correct average energy the Strutinsky method is used [7].

Another derivation of a mean-field approximation is based on the functional integral approach, where the many-body partition function is expressed as an integral over all "possible" one-body partition functions [42]:

$$Z(T) = \text{Tr} \left(e^{-H/T} \right) = \int D[\sigma] e^{-F(T, \omega; \sigma)/T} \quad (3.8)$$

Here $\sigma(\tau)$ ($0 \leq \tau \leq T^{-1}$) is a single-particle density function which depends on an imaginary time-like parameter τ . For τ -independent σ 's (the so-called "static approximation" [43,44]) the free energy $F(T, \omega; \sigma)$ is given by

$$F(T, \sigma) = -\frac{1}{2} \text{tr}(\sigma v \sigma) - T \ln \text{Tr} \left[e^{-H_\sigma/T} \right] \quad (3.9a)$$

Here H_σ is a sum of the single-particle Hamiltonians $h_\sigma^{(i)}$ where

$$h_\sigma = t + v\sigma \quad (3.9b)$$

Eqs. (3.9) describe the free energy of nucleons moving independently in a mean-field $v\sigma$. If the integral (3.8) is evaluated in the stationary phase approximation one recovers the Hartree-Fock equation (3.5). The advantage of the functional integral approach is that it allows us to go beyond the mean-field approximation by including fluctuations in σ . We shall return to this issue in Section 4.

To describe rotation of a hot nucleus we replace in (3.1) H by $H - \vec{\omega} \cdot \vec{J}$, which is the Hamiltonian in the frame rotating with angular velocity $\vec{\omega}$ [41]. Using one-body density matrices of the form (3.3) we obtain the cranked mean-field approximation where a coriolis coupling $-\vec{\omega} \cdot \vec{J}$ is included in the one-body Hamiltonian (3.9b). The free energy is now $F = F(T, \vec{\omega}; \rho)$ and can be expanded to second order in ω

$$F(T, \omega; \rho) = F(T, \omega=0; \rho) - \frac{1}{2} \sum_{i,j} I_{ij}(T; \rho) \omega_i \omega_j + \dots \quad (3.10)$$

where I_{ij} is the symmetric moment of inertia tensor. It is found that

$$I_{ij} = \int_0^{1/T} \langle J_i(\tau) J_j(0) \rangle d\tau \quad (3.11)$$

where

$$\langle J_i(\tau) J_j(0) \rangle = Z^{-1} \text{Tr} \left[e^{-H_0/T} \left(e^{H_0\tau} J_i e^{-H_0\tau} \right) J_j \right] \quad (3.12)$$

H_0 is the mean-field Hamiltonian characterized by the trial parameters ρ . If $|i\rangle$ are the corresponding single-particle states with single-particle energies ϵ_i , then [26]

$$I_{zz} = \sum_i |\langle i|J_z|i\rangle|^2 (-\partial f_i / \partial \epsilon_i) + \sum_{i \neq k} |\langle i|j_z|k\rangle|^2 \left(\frac{f_k - f_i}{\epsilon_i - \epsilon_k} \right) \quad (3.13)$$

The first contribution on the r.h.s. to I_{zz} is from the alignment of the single particle spins along the rotation axis while the second is from the collective rotation.

Open shell nuclei are usually found to be deformed in their ground state. This is a quantum mechanical effect related to the shell structure of the single-particle levels of the mean-field potential. Various mean-field calculations [6,7] indicate that when the temperature increases the nuclear shape is changing and eventually a transition to a spherical shape occurs at temperatures $T \approx 1-2$ MeV for deformed rare-earth nuclei. In the following we shall concentrate on the nuclear shape evolution with temperature and spin.

3.2 Landau Theory

The most relevant and universal features of any microscopic mean-field theory of shape transitions in hot nuclei can be described in the framework of the Landau theory [25,26]. The approach also offers a useful and economical parametrization of the results of microscopic calculations and singles out a small number of the most relevant combinations of the parameters on which the equilibrium shape depends.

The theory was introduced by Landau in 1937 [45] to describe symmetry breaking phase-transitions in statistical systems. The free energy which is a scalar is expanded in a set of trial parameters known as the order parameters. The equilibrium value of the order parameters is found by minimizing this free energy. In the symmetry-breaking phase these values of the order parameters are non-zero.

The most crucial trial parameters in the study of nuclear shapes are the quadrupole deformation parameters $\alpha_{2\mu}$ ($\mu = -2, -1, \dots, 2$). Thus instead of considering $F(T, \omega; \rho)$ we shall consider only an effective free energy $F(T, \omega; \alpha_{2\mu})$ by minimizing the former with respect to all other

shapeparameters. The symmetry-breaking phase is a deformed nucleus with $\alpha_{2\mu} \neq 0$. Thus the symmetry which is broken is the rotational invariance and the order parameters are $\alpha_{2\mu}$, the non-zero values of which characterize the degree of symmetry breaking. In the presence of rotation, the full rotational symmetry is explicitly broken by the preferred direction of the rotational axis. The remaining symmetry is that of rotations around the direction of $\vec{\omega}$, which is spontaneously broken in the phase-transition.

Since F must be a scalar, only rotationally invariant combinations of $\vec{\omega}$ and $\alpha_{2\mu}$ are allowed. The ω -independent invariants to fourth order are $(\alpha \times \alpha)^{(0)}$, $((\alpha \times \alpha)^{(2)} \times \alpha)^{(0)}$ and $(\alpha \times \alpha)^{(0)} \cdot (\alpha \times \alpha)^{(0)}$. The lowest invariants involving $\vec{\omega}$ are quadratic in ω such as $((\omega \times \omega)^{(2)} \times \alpha)^{(0)}$, $((\omega \times \omega)^{(2)} \times (\alpha \times \alpha)^{(2)})^{(0)}$ etc. To second order in $\vec{\omega}$ one can arrange these terms in the form of the expansion (3.10). We can transform from the laboratory $\alpha_{2\mu}$ to the Hill-Wheeler intrinsic parameters (β, γ) and the Euler angles $\Omega = (\psi, \theta, \phi)$. The latter characterize the orientation of the nucleus' principal frame $x'-y'-z'$ with respect to the rotation axis $\vec{\omega}$ which we choose along the z axis of the laboratory frame. The moment of inertia tensor I_{ij} is diagonal in the intrinsic principal frame and the components of $\vec{\omega}$ in that frame are

$$\begin{aligned}\omega_{x'} &= -\omega \cos\phi \sin\theta \\ \omega_{y'} &= \omega \sin\phi \sin\theta \\ \omega_{z'} &= \omega \cos\theta\end{aligned}\quad (3.14)$$

Thus (3.10) becomes

$$\begin{aligned}F(T, \omega; \alpha_{2\mu}) &= F(T, \omega=0; \beta, \gamma) - \frac{1}{2} \left[I_{x'x'} \sin^2\theta \cos^2\phi \right. \\ &\quad \left. + I_{y'y'} \sin^2\theta \sin^2\phi + I_{z'z'} \cos^2\theta \right] \omega^2\end{aligned}\quad (3.15)$$

The above Landau expansion leads to the following

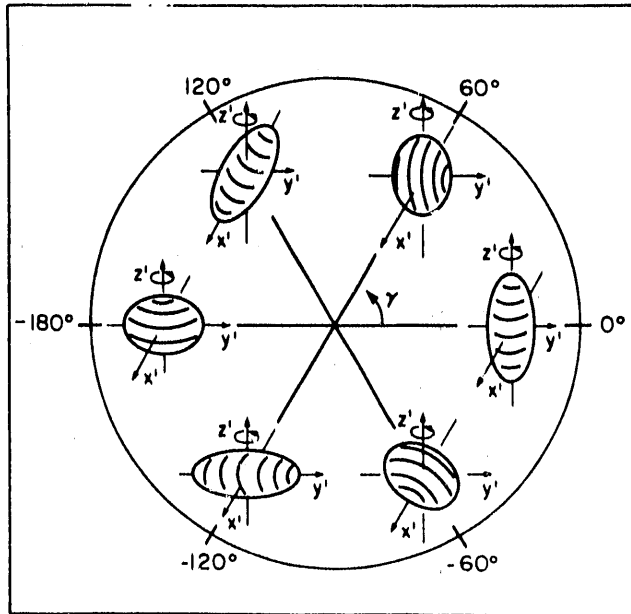
$$F(T, \omega=0; \beta, \gamma) = F_0(T) + A(T)\beta^2 - B(T)\beta^3 \cos 3\gamma + C(T)\beta^4 + \dots, \quad (3.16)$$

and

$$\begin{aligned}I_{z'z'}(T; \beta, \gamma) &= I_0(T) - 2R(T)\beta \cos\gamma + 2I_1(T)\beta^2 + 2D(T)\beta^2 \sin^2\gamma + \dots, \\ I_{x'x'}(T; \beta, \gamma) &= I_{z'z'}(T; \beta, \gamma - 2\pi/3), \\ I_{y'y'}(T; \beta, \gamma) &= I_{z'z'}(T; \beta, \gamma + 2\pi/3).\end{aligned}\quad (3.17)$$

The temperature-dependent coefficients $F_0, A, B, C, I_0, R, I_1$ and D are

Fig. 1. The (β, γ) plane of shapes of deformed nuclei rotating around a principal axis z' .



phenomenological parameters which are not determined by the Landau theory. However, the topography of the free energy surface (3.15) - (3.17) depends only on certain combinations of these parameters as we shall see below.

The equilibrium configuration is found by minimizing the free energy with respect to $\alpha_{2\mu}$. Minimizing first with respect to the orientation Ω , one obtains as a necessary condition for the minimum the standard result that the nucleus must be oriented such that one of its principal axes, say z' , is directed along $\vec{\omega}$. We then allow (β, γ) to cover the full plane ($0 \leq \beta < \infty$; $-180^\circ \leq \gamma \leq 180^\circ$). This (β, γ) plane of shapes of deformed nuclei rotating around a principal axis z' is shown in Fig. 1. The sufficient conditions for a minimum require further that the rotation is around the axis with the largest moment of inertia, namely

$$I_{z'z'} > I_{x'x'}, I_{y'y'} \quad (3.18)$$

After minimizing with respect to the angles, the free energy (3.15) becomes

$$F(T, \omega; \alpha_{2\mu}) = F_0(T) + A(T)\beta^2 - B(T)\beta^3 \cos 3\gamma + C(T)\beta^4 - \frac{1}{2} I_{zz}(T; \beta, \gamma) \omega^2 \quad (3.19)$$

where $I_{z'z'}$ is given by (3.17).

For stability one must require $C(T) > 0$, and nuclei with deformed ground state have $A(T) < 0$ at low temperatures. The prolate-oblate asymmetry requires $B(T) \neq 0$. For definiteness, we will discuss the more frequently occurring prolate case $B(T) > 0$. When T increases $A(T)$ changes sign at some temperature which is usually between 1 and 2 MeV for the deformed rare-earth nuclei. In the case $D=0$ (rigid body moment of inertia)

the relevant dimensionless combinations are the reduced temperature

$$\tau = \frac{AC}{B^2} \quad (3.20)$$

and ω/ω_c where

$$\omega_c = \frac{9}{16} (B/C) (B/R)^{1/2} \quad (3.21)$$

is a critical angular velocity.

In these reduced variables a universal phase diagram emerges. Minimizing (3.19) one finds that at negative values of τ , i.e. at low T and not too large ω , there are seven extrema in the entire (β, γ) plane. They are located symmetrically due to the $\gamma \leftrightarrow -\gamma$ symmetry of the free energy. For $D=0$, the condition $I_{z'z'} > I_{x'x'}, I_{y'y'}$ (see Eq. (3.18)) selects those extrema which falls in the sector $|\gamma| > 120^\circ$ only. At negative τ , there are three such extrema, one oblate ($\gamma = -180^\circ$) and two triaxial related by the $\gamma \leftrightarrow -\gamma$ symmetry. Only one of the latter should be considered, since they both give the same shape up to a rotation by 90° around the z axis. We choose to work in the sector $-180^\circ \leq \gamma \leq -120^\circ$. For $B > 0$ and $\tau < 0$, the triaxial configuration is the stable equilibrium shape and the oblate is a saddle point.

When τ increases towards positive values for fixed ω , one finds a

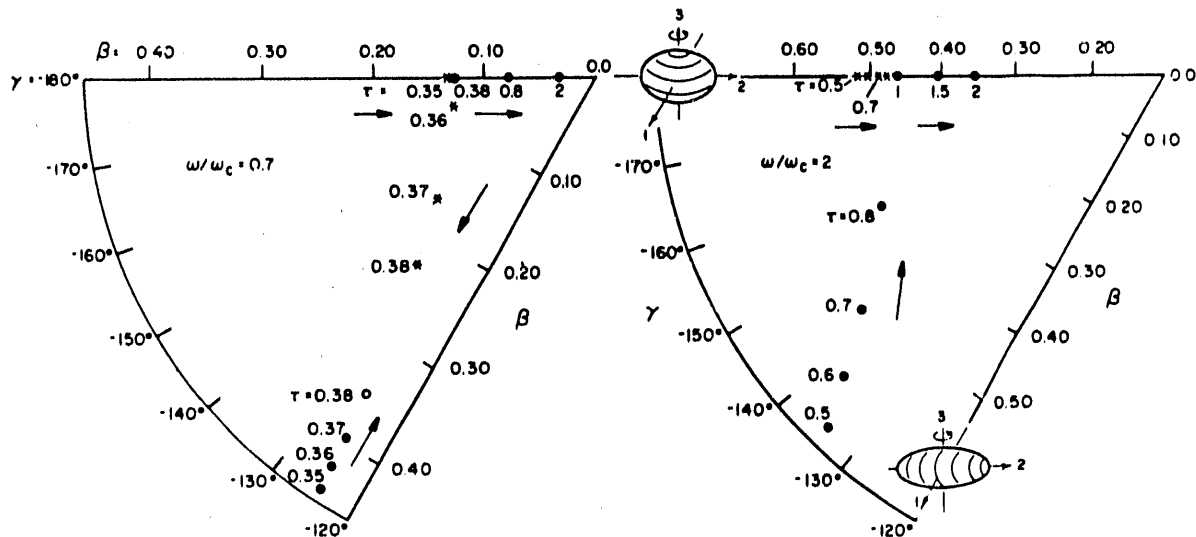


Fig. 2. Motion of the extrema in the β - γ plane with changing τ and fixed ω/ω_c . On the right a second-order transition is shown for $\omega/\omega_c=2$ with dots denoting a global minimum and asterisks a saddle point. On the left is a first-order transition for $\omega/\omega_c=0.7$ where open circles denote a local minimum.

behavior which depends on whether ω is smaller or larger than ω_c (see Eq.(3.21)). For fixed $\omega/\omega_c > 1$ and τ increasing (see r.h.s. of Fig. 2), the triaxial minimum moves towards the oblate saddle point and coincides with it when τ reaches

$$\tau = \frac{9}{8} [1 - (\omega/4\omega_c - 1)^2] \quad (3.22)$$

When τ increases above (3.22), the oblate shape becomes the only stable minimum. This is a second-order phase-transition where the order parameter (at the minimum) changes continuously. When $\omega/\omega_c < 1$ (see l.h.s. of Fig. 2) and τ reaches (3.22), the oblate saddle point turns into a local minimum but the triaxial minimum is still separated from it. Instead, when τ increases past (3.22) a new triaxial saddle point emerges out of the oblate and moves towards the old. The two coalesce and disappear when τ reaches

$$\tau = \frac{9}{32} \left(1 + \frac{3}{4} \omega^2/\omega_c^2 \right) \quad (3.23)$$

Above the τ in (3.23) only the oblate minimum remains. The phase transition from the triaxial minimum to oblate minimum occurs for τ between (3.22) and (3.23), when the free energies of these two minima are equal. This is then a first-order transition. The motion of the extrema is demonstrated in Fig. 2 for $\omega < \omega_c$ and for $\omega > \omega_c$. Fig. 3 is a phase diagram in the τ - ω/ω_c plane for $D=0$ nuclei. The solid line for $\omega > \omega_c$ is the transition line of the second-order transitions. For $\omega < \omega_c$, there is a "coexistence" region whose boundaries are defined by (3.22) and (3.23). It is shown in

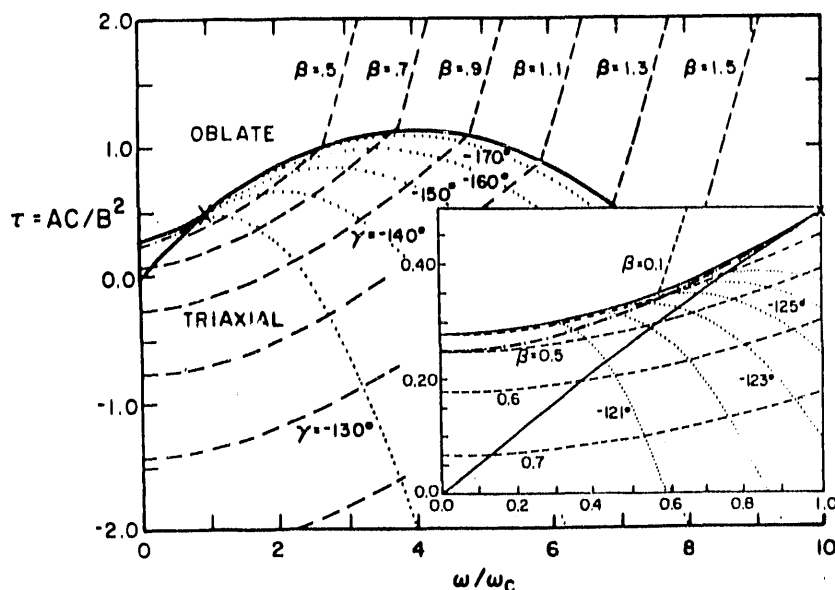


Fig. 3. Phase-diagram in the variables τ and ω/ω_c . The tricritical point is denoted by an \times . The solid line separates the triaxial phase from the non-collective oblate phase. Insert: the first order transition region.

more detail in the insert of Fig. 3. The point $\omega=\omega_c$, $\tau=\tau_c=63/128$ separates the first order from the second order transitions and is known as a tricritical point [46]. Also shown in Fig. 3 are contour lines of β (in units of B/C) and γ . We see that near the tricritical point the shape changes rapidly from almost prolate to oblate.

3.3. Microscopic Calculations

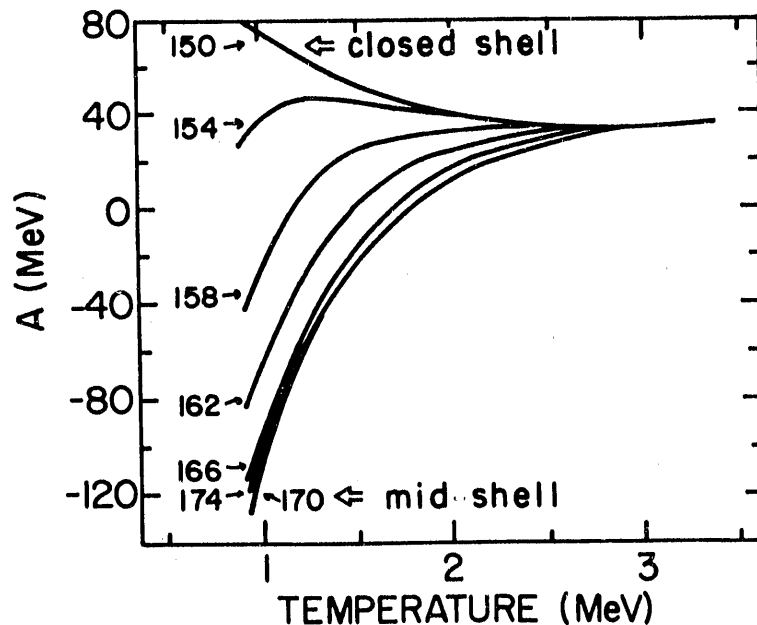
The unfolding of the universal phase-diagram to the experimentally accessible variables, excitation energy and spin, requires the knowledge of the Landau parameters in the expansion (3.15)-(3.17). We have performed [47] microscopic calculations of the free energy surfaces of various nuclei and mapped them on the Landau expansion in order to determine the parameters A(T), B(T), C(T) etc.

The surfaces are calculated using cranked Nilsson-Strutinsky procedure for rotations along a principal axis z. The frequencies ω_k of the deformed harmonic potential well were parametrized according to Hill and Wheeler:

$$\omega_k = \omega_0 \exp \left[- \sqrt{\frac{5}{4\pi}} \beta \cos \left(\gamma - \frac{2\pi}{3} k \right) \right] \quad (3.24)$$

For $\omega=0$ (no rotation) pairing is also included using a BCS monopole pairing force. In the liquid-drop energy we have allowed for large deformations by taking the exact Coulomb and surface energies expressed as elliptic integrals. For a given nucleus and a temperature T we can determine based on the expansion (3.15), the surfaces $F(T; \omega=0, \beta, \gamma)$ and $I_{zz}(T; \beta, \gamma)$. Using (3.16), we find F_0 , A, B and C. Using (3.17) we determine the moment of

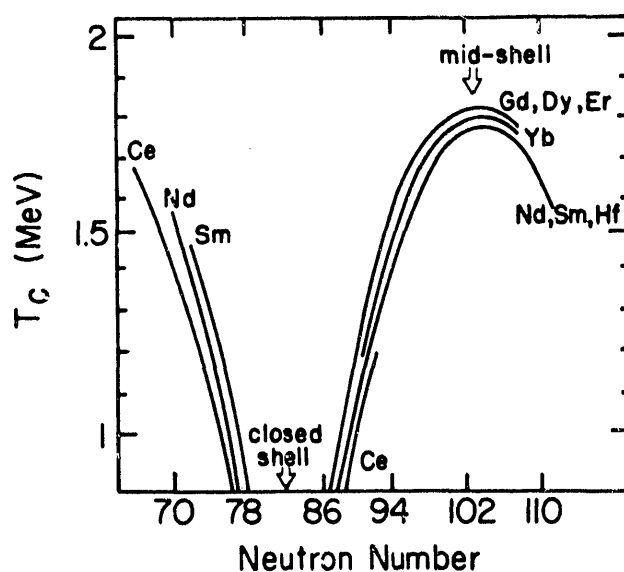
Fig. 4. The Landau parameter A(T) for various erbium isotopes as calculated microscopically. All curves converge to a common value ≈ 30 MeV for $T \geq 3$ MeV.



inertia coefficients I_0, R, I_1 and D . The complete Landau expansion at any ω and $\alpha_{2\mu}$ is then given by (3.15). The Landau expansion (3.15)-(3.17) reproduces well the microscopic surfaces for $T \geq 1$ MeV and moderate spins.

The Landau parameters have been determined [47] for all even-even rare-earth nuclei. They are found to obey simple systematics as a function of N and Z of the nucleus. Fig. 4 shows, for example, $A(T)$ for different erbium isotopes in the temperature range $T \geq 0.8$ MeV. A is the most crucial parameter in the Landau theory since the prolate to spherical shape transition at $\omega=0$ occurs near the temperature where A changes sign. We see from Fig. 4 that the value of A is sensitive to shell effects. For mid-shell nuclei, which are strongly deformed in their ground state, A starts from values large in magnitude and negative, and increases monotonically with T towards positive values. Such nuclei undergo shape transition from almost prolate to oblate at $\omega=0$. For nuclei near shell closure, A starts positive and decreases monotonically while never becoming negative. Such nuclei start and stay spherical but become softer with increasing T . Above $T \approx 3$ MeV all rare-earth nuclei have approximately the same A (≈ 30 MeV) due to the disappearance of shell effects. Fig. 5 shows the critical temperature T_c versus neutrons number for the even-even rare-earth nuclei. T_c is very close to the temperature at which $r=r_c$. On the phase-diagram of deformed nuclei the value of T_c determines the position of the line of triaxial to oblate shape transitions. The systematic of T_c is strikingly simple. For each family of isotopes between two closed neutron shells the values of T_c fall on an inverted parabola-like curve whose maximum is at mid-shell. The curve drops rapidly towards shell closure. This is of course consistent with the A systematics of Fig. 4. For various families of isotopes the parabola-like curves are arranged like onion shells where the innermost shells correspond to isotopes near proton shell closure at $Z=50$ and 82 , and the outermost shells are in the region of proton mid-shell, ${}_{66}\text{Dy}$. The largest critical temperature of $T_c \sim 1.85$ MeV is found in mid-neutron shell isotopes of Gd, Dy and Er.

Fig. 5. The critical temperature T_c as a function of neutron number for even-even rare-earth nuclei. The maximal value of T_c occurs near the neutron mid-shell ($N=104$) for a given isotope family and near the proton mid-shell ($Z=66$) among the various families.



Finally, we consider the angular momentum J_c which corresponds to $\omega = \omega_c$ i.e. $J_c = I_{zz} \omega_c$. The critical spin J_c is shown in Fig. 6 for various rare-earth isotope families. We note that since $\omega_c \sim B^{3/2}/C$ we expect the J_c systematics to be dominated by the B-systematics. B on the other hand governs the prolate-oblate free energy difference which is $\Delta F = (24/256)(B^4/C^3)$. One can apply Hill and Wheeler's "thirds of the shell" rule [48] according to which prolate ground state deformation dominates in the first two-thirds of the shell while oblate deformation is typical for the last third. It is thus expected that $B \sim 0$ around two-thirds of a filled shell and is maximal around one-third of a filled shell. The behavior of J_c in Fig. 6 tends to support the foregoing analysis with J_c rising rapidly from neutron shell closure at 82 to a maximum in the neighborhood of the end of the first third of the shell (N=96) and then proceeding to fall towards zero at the end of the second third of the shell (N=112). An approximate proton "thirds of the shell" rule is also observed by inspecting the various curves in Fig. 6. The proton shell closure is 50 and 82, so that the outermost curves correspond to nuclei with 60-62 protons (Nd and Sm), while the innermost curves correspond to 70-72 protons (Yb and Hf). In general the values of J_c are relatively small ($\leq 10-15\hbar$), indicating that the transitions are very close to being second-order.

Using the Landau parameters it is possible, for the nucleus under consideration, to unfold the universal phase-diagram to the physical

Fig. 6. The angular momentum J_c at the tricritical point vs. neutron number for rare-earth nuclei.

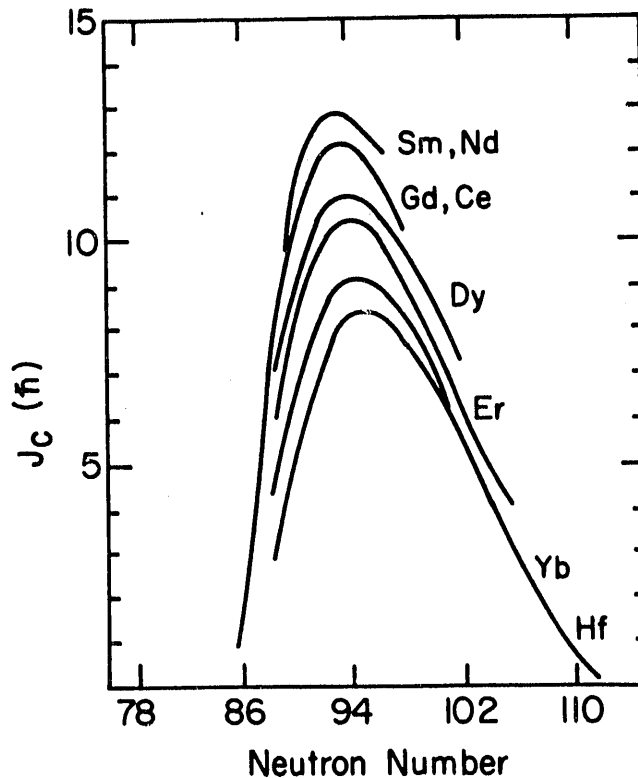
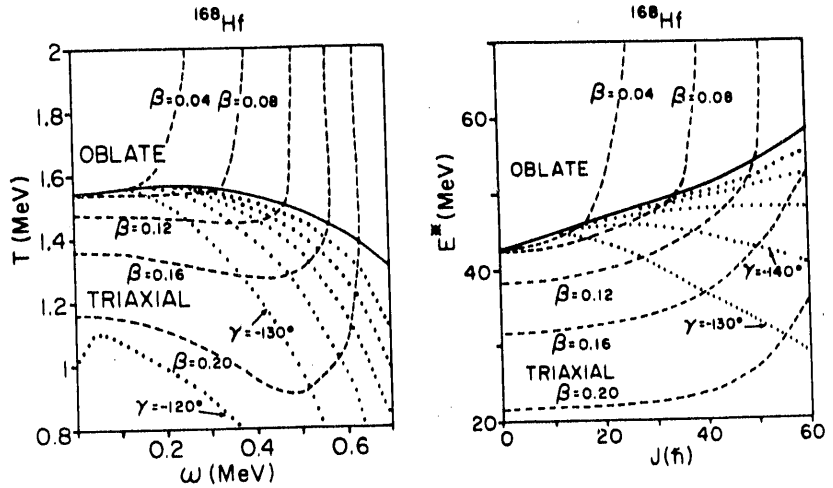


Fig. 7. Phase diagram for ^{168}Hf in intensive variables (T, ω) (left) and extensive variables (E^*, J) (right).



variables (E^*, J) . An example is shown in Fig. 7 for ^{168}HF .

4. Fluctuations

Since the nuclear system is finite, fluctuations away from the mean-field configuration are important. According to Eq. (3.8) for the nuclear many-body partition function, all possible one-body potentials $v\sigma$ should be admitted each with a probability given by the Boltzmann factor

$$P[\sigma] \propto \exp[-F(T, \omega; \sigma)/T] \quad (4.1)$$

with the free energy given by (3.9). For the finite nucleus P is maximal for $\sigma = \sigma_{\text{eq}}$ (the HF solution ρ of (3.5)) but is non-negligible for $\sigma \neq \sigma_{\text{eq}}$.

It is possible to evaluate the small amplitude fluctuations by approximating (4.1) by a Gaussian in $\sigma - \sigma_{\text{eq}}$, with a width given by the second variation of the exponent. We then obtain the temperature-dependent RPA approximation [42]. This approximation is not sufficient when some of the directions are "soft," in which case the integral (3.8) in these directions should be evaluated exactly [43].

We have developed a macroscopic approach to fluctuations [29,32] in the Landau framework in which fluctuations in the order parameters are treated exactly. In our case we assume a unified theory of shape fluctuations in which all five $\alpha_{2\mu}$ are included. The probability of finding a nucleus in a "state" with deformation $\alpha_{2\mu}$ is given by [49]

$$P[\alpha_{2\mu}] = Z^{-1} \exp[-F(T, \omega; \alpha_{2\mu})/T] \quad (4.2)$$

where

$$Z(T, \omega) = \int D[\alpha] \exp(-F/T) \quad (4.3)$$

is the nuclear partition function. The free energy F in (4.2) is given by the general Landau expansion (3.15)-(3.17). This theory takes into account large amplitude fluctuations in $\alpha_{2\mu}$. The phase-space volume element $D[\alpha_{2\mu}]$ is chosen to be the one which treats all five $\alpha_{2\mu}$ uniformly, namely the unitary invariant metric

$$D[\alpha_{2\mu}] = \prod_{\mu} d\alpha_{2\mu} = \beta^4 |\sin 3\gamma| d\beta d\gamma d\Omega \quad (4.4)$$

It should be noted that our theory takes into account fluctuations not only in the intrinsic shape β, γ but also in the nuclear orientation Ω relative to the rotation axis $\hat{\omega}$. Previous analyses of shape fluctuations have neglected the latter.

The importance of (4.2) is in its use of calculating expectation values of any physical observable X (which is shape-dependent)

$$\langle X \rangle = \int D[\alpha_{2\mu}] P[\alpha_{2\mu}] X(\alpha) \quad (4.5)$$

In subsequent chapters we shall compare the value of $\langle X \rangle$ obtained by (4.5) where shape fluctuations are included with the value $X(\alpha_{eq})$ predicted by the mean-field theory, for several physical observables X . We shall see that they are quite different.

5. Giant Dipole Resonances in Hot Rotating Nuclei

The giant dipole resonance (GDR) built on nuclear excited states was observed in recent years at several laboratories, and is one of the major probes of shapes and properties of hot rotating nuclei [18-24].

In cold nuclei ($T=0$) the frequency of the giant resonance vibration is inversely proportional to the length of the semi-axis along which the vibration occurs [50,51]. Therefore in deformed nuclei the resonance splits and from the amount of splitting it was possible to determine its deformation. A similar technique was used to determine the shape of hot rotating nuclei [18-24]. However, due to shape fluctuations around the equilibrium shape, the relationship between the equilibrium nuclear shape and the GDR spectral shape is more complex. It has been recognized by several authors that thermal shape fluctuations play an important role in determining the width of the resonance [28,30,31].

Microscopic theories of GDR underestimate the width of the GDR [17]. The finite-temperature RPA also predicts that the GDR is rather insensitive to temperature. However, recent measurements indicate strong dependence of the width on temperature for spherical nuclei [18]. By using [17] a phenomenological escape width, one can increase the calculated width, but the spectral shape is still in disagreement with the observed one. We have developed a macroscopic approach [29,32] to the GDR in hot nuclei in the framework of the Landau theory. All parameters are determined from the properties of the $T=0$ GDR. In this theory unified large-amplitude fluctuations in the order parameters ($\alpha_{2\mu}$) play an important role. It is

the first theory which is able to reproduce both the observed cross-section and the angular anisotropy of the GDR γ -rays emitted from the hot nucleus [33,34].

5.1 Macroscopic Theory

In this section we shall derive an exact expression for the GDR absorption cross-section $\sigma(\epsilon)$ and the angular anisotropy coefficient $a_2(\epsilon)$ (see definition below) in terms of the dipole temporal autocorrelation function evaluated at equilibrium.

The differential cross-section for a nucleus of energy E and spin J to emit an electric dipole γ -ray of energy ϵ and direction Θ with respect to an axis to be specified below is

$$\frac{d\Gamma_{em}}{d\epsilon d\Omega} = \frac{1}{2\pi\hbar} \left(\frac{\epsilon}{\hbar c}\right)^3 \frac{1}{\rho(\epsilon, J)} \sum_{\substack{i, f \\ \mu, M_i}} |\langle f J M_f | D_\mu | i J M_i \rangle|^2 \delta(E-E_i) \delta(E'-E_f) F_\mu(\Theta), \quad (5.1)$$

where $E'=E-\epsilon$. The sum represents an average over all initial states of energy E and spin J and a sum over all final states of energy E' . Here $\rho(E, J)$ is the initial level density and D_μ is the dipole operator. The angular functions $F_\mu(\Theta)$ are given by

$$F_\mu(\Theta) = |d_{\mu, 1}^1(\Theta)|^2 + |d_{\mu, -1}^1(\Theta)|^2, \quad (5.2)$$

where d^1 are the Wigner matrices for spin 1. Eq. (5.1) can be rewritten in the following way:

$$\frac{d\Gamma_{em}}{d\epsilon d\Omega} = \frac{1}{(2\pi\hbar)^2} \left(\frac{\epsilon}{\hbar c}\right)^3 \sum_{\mu} \int_{-\infty}^{\infty} dt e^{i\epsilon t/\hbar} \langle D_\mu^\dagger(t) D_\mu(0) \rangle_{E, J} F_\mu(\Theta), \quad (5.3)$$

where $D_\mu(t)$ is the dipole operator in the Heisenberg representation and the average $\langle \dots \rangle_{E, J}$ is over the microcanonical ensemble

$$\langle X \rangle_{E, J} = \text{Tr} [X \delta(E-H) P_J] / \text{Tr} [\delta(E-H) P_J] \quad (5.4)$$

In Eq. (5.4) P_J is the projection on states with spin J .

As usual we replace in (5.3) the microcanonical average by a canonical average $\langle D_\mu^\dagger(t) D_\mu(0) \rangle_{T, \omega}$ where

$$\langle \chi \rangle_{T, \omega} = \text{Tr} [X e^{-(H - \vec{\omega} \cdot \vec{J})/T}] / \text{Tr} e^{-(H - \vec{\omega} \cdot \vec{J})/T} \quad (5.5)$$

In doing so, we have chosen a preferred direction $\vec{\omega}$. Choosing this direction to be the z-axis, we are measuring the γ -ray with respect to the rotation axis $\vec{\omega}$, i.e. approximately with respect to the spin direction. From Eqs. (5.2) and (5.3) we find that the angular distribution of the γ -rays can be written as

$$\hbar \frac{d\Gamma_{em}}{d\epsilon d\Omega} = \frac{1}{4\pi} \left(\frac{\epsilon}{\pi \hbar c} \right)^2 \sigma(\epsilon) [1 + a_2(\epsilon) P_2(\Theta)] \quad (5.6)$$

where

$$\sigma(\epsilon) = \frac{2\pi\epsilon}{3\hbar^2 c} \int_{-\infty}^{\infty} dt e^{i\epsilon t/\hbar} \langle D_{\mu}^{\dagger}(t) D_{\mu}(0) \rangle \quad (5.7)$$

and

$$a_2(\epsilon) = \frac{1}{2} - \frac{3}{2} \frac{\int_{-\infty}^{\infty} dt e^{i\epsilon t/\hbar} \langle D_0^{\dagger}(t) D_0(t) \rangle}{\int_{-\infty}^{\infty} dt e^{i\epsilon t/\hbar} \sum_{\mu} \langle D_{\mu}^{\dagger}(t) D_{\mu}(0) \rangle} \quad (5.8)$$

$\sigma(\epsilon)$ is the GDR absorption cross-section and a_2 is known as the angular anisotropy parameter. If the angular distribution is measured with respect to the beam axis, then, assuming it is perpendicular to the spin direction, we have to multiply (5.8) by $(-1/2)$. In the following and in all calculations we shall use this a_2 unless otherwise specified.

5.2. Fixed Deformation

In order to calculate the dipole correlation functions in (5.7) and (5.8) we first need to evaluate them for a constant deformation $\alpha_{2\mu}$. In Section 5.3 we will show how to take into account the fluctuations of $\alpha_{2\mu}$ at finite temperature. In the absence of rotations ($\omega=0$) the tensor $\langle D_{\mu}^{\dagger}(t) D_{\mu}(0) \rangle$ is diagonal in the intrinsic frame of the nucleus. In that frame $\alpha_{2\mu}$ is also diagonal and is defined in terms of the Hill-Wheeler coordinates β, γ and the Euler angles Ω which determine the orientation of the nucleus relative to the rotation axis $\vec{\omega}$. Rotation matrices relate the correlation tensor in the intrinsic frame to that in the laboratory frame. We adopt the common assumption that the resonant energies of the three giant dipole oscillatory

modes are inversely proportional to the semi-axis lengths of the ellipsoid representing the nuclear shape [50,51]

$$E_j^0 = E_0 \frac{R_0}{R_j} = E_0 \exp \left[-\sqrt{\frac{5}{4\pi}} \beta \cos(\gamma - \frac{2\pi}{3} j) \right] ; \quad (j=1,2,3) \quad (5.9)$$

and that the Fourier transform of the correlation tensor (multiplied by the additional factor of ϵ in (5.7)) is proportional to a Lorentzian,

$$f_j(\epsilon) = \frac{\Gamma_j \epsilon^2}{(\epsilon^2 - E_j^2)^2 + \Gamma_j^2 \epsilon^2} \quad (5.10)$$

In (5.10) the natural frequencies are $E_j(\omega=0) = E_j^0$ as given by (5.9) and Γ_j are the decay widths along the j -th intrinsic axis; E_0 is a constant which varies from nucleus to nucleus. Equation (5.9) follows from the nuclear hydrodynamics model where giant resonances are oscillations in the proton and neutron fluid densities and thus have wavelengths nearly proportional to the length of the semi-axis along which the oscillations occur [50,51]. Equation (5.10) follows from assuming that the dipole in the intrinsic principal frame is damped as is the displacement of a harmonic oscillator in an external field. The strength of the Lorentzian (5.10) is fixed by the classical sum rule [50].

In the presence of rotation ($\omega \neq 0$) the Coriolis and centrifugal forces shift the normal frequencies from E_j^0 to $E_j(\vec{\omega})$ and make the correlation tensor nondiagonal in the intrinsic frame. However, there exists a canonical transformation to normal coordinates in which the correlation tensor is diagonal. To find that transformation we model the giant dipole oscillator by a rotating deformed three-dimensional harmonic oscillator. The Hamiltonian in the intrinsic rotating frame is

$$H(d,p) = \frac{1}{2} \vec{p}^2 + \frac{1}{2} \sum_i E_i^2 d_i^2 - \vec{\omega} \cdot (\vec{d} \times \vec{p}) \quad (5.11)$$

where \vec{d} is the giant dipole operator in the intrinsic frame and \vec{p} is its conjugate momentum. In Ref. 32 we have shown that the correlation function in this frame can be written in terms of the raising and lowering operators for the three normal modes, a_s^\dagger and a_s , and a matrix \mathbb{M} which relates the normal coordinates to the intrinsic ones:

$$\langle d_o^\dagger(t) d_r(0) \rangle = \sum_{st} \mathbb{M}_{os}^* \mathbb{M}_{rt} \langle a_s(t) a_t^\dagger(0) \rangle \quad (5.12)$$

The matrix \mathbb{M} depends on ω , β and γ (through E_j^0) and Ω . As in the nonrotating case, the Fourier transform of the correlation tensor in the "normal" frame, $\langle a_s(t) a_t^\dagger(0) \rangle$, is assumed to be diagonal and to have the Lorentzian form (5.10) but now with shifted E_j .

The relationship between the dipole operator in the laboratory frame

(D_μ) and in the intrinsic rotating frame (d_μ) is simply

$$D_\mu(t) = e^{-i\tilde{\omega}t \cdot \mathbf{J}/\hbar} \sum_\lambda D_{\mu\lambda}(\Omega) d_\lambda(t) e^{+i\tilde{\omega}t \cdot \mathbf{J}/\hbar} \quad (5.13)$$

where $\Omega = (\psi, \theta, \phi)$ are the Euler angles and D is the Wigner rotation matrix for spin 1.

We find that the cross-section in the laboratory frame is given by

$$\sigma(\epsilon; \beta, \gamma, \Omega) = \frac{4\pi e^2 \hbar}{mc} \frac{Z N}{A} \sum_{j=1}^3 \left[S_j^{(0)} f_j(\epsilon) + S_j^{(-)} f_j(\epsilon + \hbar\omega) + S_j^{(+)} f_j(\epsilon - \hbar\omega) \right] \quad (5.14)$$

while the angular anisotropy is

$$a_2(\epsilon; \beta, \gamma, \Omega) = \frac{3}{4} \frac{\sum_j S_j^{(0)} f_j(\epsilon)}{\sum_j S_j^{(0)} f_j(\epsilon) + S_j^{(-)} f_j(\epsilon + \hbar\omega) + S_j^{(+)} f_j(\epsilon - \hbar\omega)} - \frac{1}{4} \quad (5.15)$$

Here $S_j^{(0, \pm)}$ are the resonance strengths in units of the classical sum rule:

$$S_j^{(\pm)} = \frac{1}{6} \sum_{\mu\nu} \left[(\delta_{\mu\nu} - n_\mu n_\nu) \operatorname{Re}(\mathfrak{M}_{\mu j}^* \mathfrak{M}_{\nu j}) \pm \sum_\lambda \epsilon_{\lambda\mu\nu} n_\lambda \operatorname{Im}(\mathfrak{M}_{\mu j}^* \mathfrak{M}_{\nu j}) \right]$$

$$S_j^{(0)} = \frac{1}{3} \sum_{\mu\nu} n_\mu n_\nu \operatorname{Re}(\mathfrak{M}_{\mu j}^* \mathfrak{M}_{\nu j}) \quad (5.16)$$

Here \hat{n} is a unit vector along the rotation axis and n_μ are its components in the principal intrinsic frame. $\epsilon_{\lambda\mu\nu}$ is the completely antisymmetric tensor. It is seen that σ is generally the sum of nine Lorentzians in the laboratory frame (which are non-degenerate for triaxial nuclei rotating around an axis which is not principal). For noncollective nuclear rotations all but two sets of the Lorentzians coincide; all but five sets of lines coincide when the angular velocity is parallel to a principal axis. For rare-earths the splitting is usually small ($\omega \lesssim 0.5$ MeV) compared to the widths of the Lorentzians. For lighter nuclei it may be more significant—due to the fact that ω can be as large as 2-3 MeV for moderate spins.

The cross-section (5.14) and a_2 in (5.15) will be completely specified as soon as the widths Γ_j in (5.10) are defined. We use for these widths a power-law [52] dependence on the resonance energy

$$\Gamma_j = \Gamma_0 \left(\frac{E_j}{E_0} \right)^\delta \quad (5.17)$$

where Γ_0 depends on the nucleus under consideration. Equation (5.17) is consistent with the experimental dependence of the ground-state GDR widths on deformation in heavy nuclei. It can also be derived using surface dissipation models. In such a theory the width, in units of Γ_0 , is reduced to a purely geometrical quantity expressed as an elliptic integral [53]. It is well approximated by a power law with $\delta=1.6$. The only free parameters (E_0, Γ_0, δ) which are assumed to depend weakly on T are determined from the zero temperature properties of the nucleus as discussed in Ref. 32.

If the effect of the Coriolis force on the eigenfrequencies is neglected ($\omega \rightarrow 0$), it is possible to derive an analytic expression for $\sigma(\epsilon)$ and a_2 as a function of the orientation (θ, ϕ). In this approximation, the correlation tensor $\langle d_i^\dagger(t) d_j(0) \rangle$ ($i, j=1, 2, 3$) is diagonal and from Eqs. (5.7) and (5.8) we find

$$\sigma \propto f_x + f_y + f_z \quad (5.18)$$

and

$$a_2 = -\frac{1}{2} \frac{(f_x + f_y)/2 - f_z}{f} \frac{3 \cos^2 \theta - 1}{2} + \frac{3}{8} \frac{f_x - f_y}{f} \sin^2 \theta \cos 2\phi \quad (5.19)$$

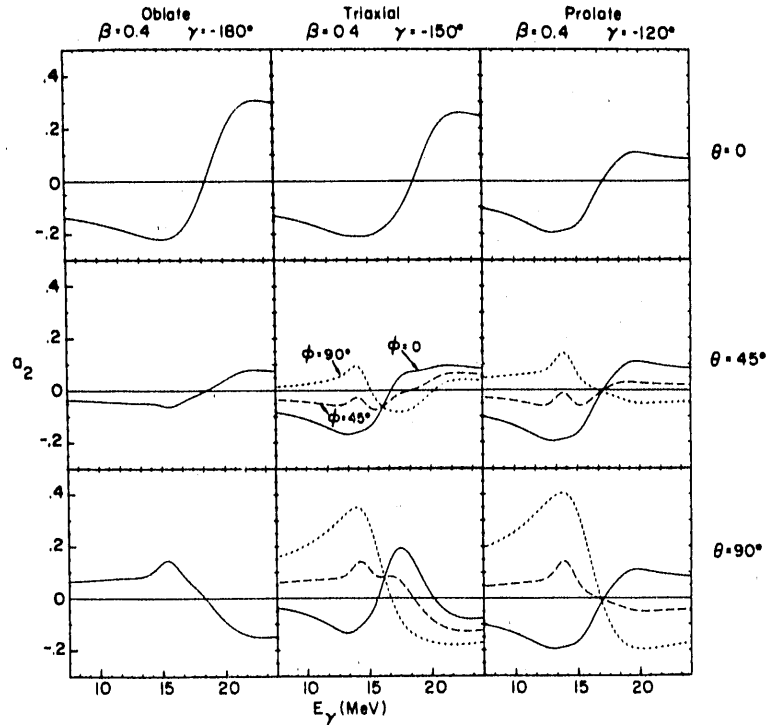
where $f = f_x + f_y + f_z$ and f_i ($i=x, y, z$) are the Fourier transforms of $\langle d_i^\dagger(t) d_i(0) \rangle$ as given by Eq. (5.10). Notice that a_2 in (5.19) is the one with respect to the beam axis.

Here a_2 is independent of the Euler angle ψ . For axially symmetric shapes (with symmetry axis z) $f_x = f_y$ and a_2 is then also independent of ϕ . It is seen that while σ is independent of orientation (in this approximation) a_2 is very sensitive to orientation. This is demonstrated in Fig. 8.

5.3 Thermal Fluctuations (Adiabatic Theory)

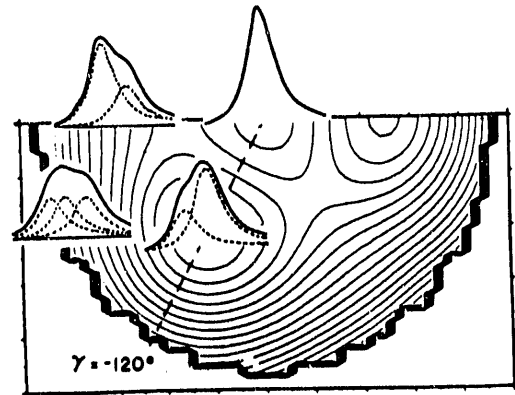
If the fluctuations in the shape are slow enough then the equilibrium averages in (5.7) and (5.8) are done according to (4.5) by averaging the contribution from a fixed $\alpha_{2\mu}$ over all possible intrinsic shapes and shape orientations. This is demonstrated in Fig. 9 for the GDR cross-section.

Fig. 8. The dependence of a_2 on orientation (θ, ϕ) for different intrinsic shapes.



To compare our theory with experiment we have applied [33] it to three cases for which precision measurements were recently taken [34]: ^{90}Zr at $T=1.6$ MeV, $J=10\hbar$; ^{90}Zr at $T=1.7$ MeV, $J=22\hbar$; and ^{92}Mo at $T=2$ MeV, $J=33\hbar$. The free energy surfaces were constructed from a cranked Nilsson-Strutinsky Hamiltonian. The cranking calculations were done only for $\bar{\omega}$ parallel to a principal axis from which the moments of inertia were determined as a function of β and γ . The free energy for a general orientation Ω is then determined by the expression (3.15). We have calculated the phase-diagrams of these nuclei and found that at the equilibrium configuration $\omega=0.47$, 1.03 and 1.36 MeV respectively in each of

Fig. 9. GDR cross-sections are shown at various deformations in the (β, γ) plane. The observed cross-section is obtained by averaging according to (4.5).



the above three cases. The equilibrium shape is a non-collective oblate ($\gamma=-180^\circ$; $\theta=0$) whose deformation increases with spin; $\beta=0.02$, 0.08 and 0.16 , respectively. When the metric (4.4) is included with the distribution (4.2), the resulting most probable shapes are triaxial ($\gamma\approx-150^\circ$) and their deformation is significantly larger; $\beta=0.24$, 0.31 and 0.46 , for the above three cases. From the ground-state GDR data in ^{90}Zr and ^{92}Mo we have determined $E_0=16.82$ MeV and $\Gamma_0=5$ MeV. Both σ and a_2 were then calculated from (5.7) and (5.8) where fluctuations in the intrinsic deformation (β, γ) were included as well as those in the orientation (θ, ϕ).

The results are shown by the solid curves in Fig. 10. They agree very well with the experiment [34] shown by the error bars. In particular, the theory reproduces accurately the observed broadening of σ at finite temperature. In judging the quality of the agreement between the calculated and experimental a_2 , the region $E_\gamma \lesssim 11$ MeV should be disregarded since there the γ -rays from daughter nuclei contaminate the signal. The latter have lower spin and energy and tend to drive the observed a_2 to zero. Also, at the high energy side we are at the tail of the resonance and their error bars are large. Thus the range to consider in Fig. 10 for the a_2 fit is $11 \lesssim E_\gamma \lesssim 20$ MeV.

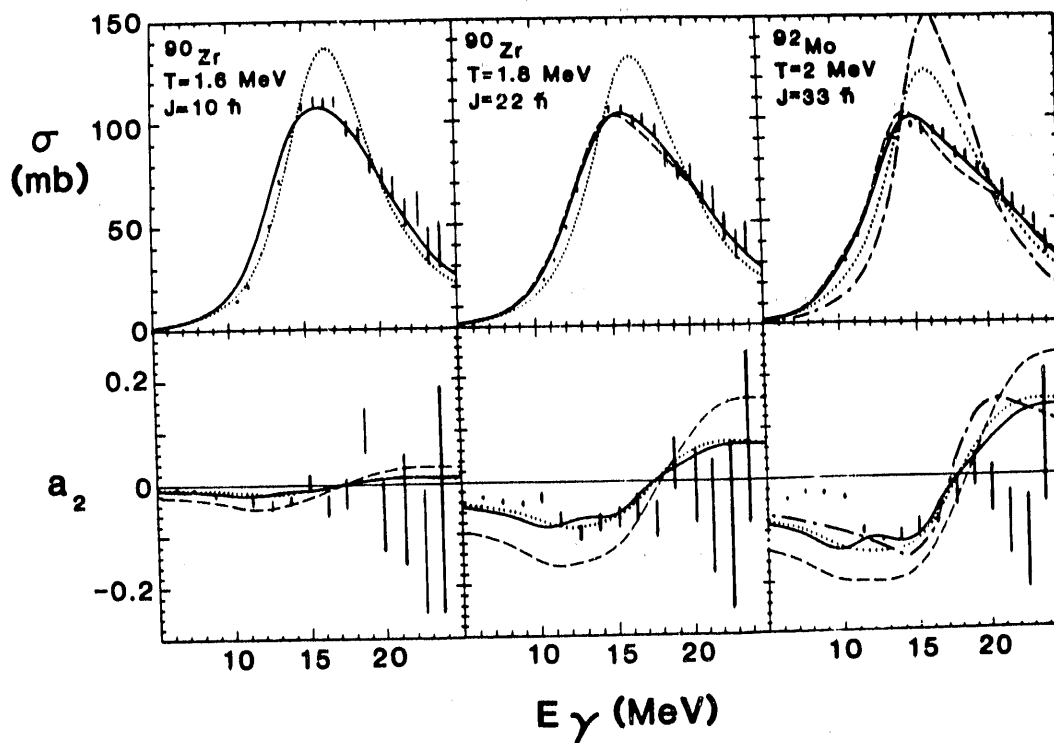


Fig. 10. The GDR absorption cross-section σ (top row) and the angular anisotropies a_2 (bottom row) versus γ -ray energy E_γ for ^{90}Zr and ^{92}Mo . The error bars are the experimental data. The following calculations are shown: with orientation fluctuations (solid lines) and without orientation fluctuations (dashed lines) using the metric (4.4); without the orientation fluctuations using the metric (5.20) (dotted lines) and the mean-field results (dashed-dotted lines in the right column).

The dashed lines in Fig. 10 are the results of similar calculations but with no orientation fluctuations. The metric (4.4) is used. Comparing them with the solid lines, we see that the effect of the orientation fluctuations on the cross-section is small. Only in the high spin case ($J=33 \hbar$) is this effect measurable, and does it provide a correction at the high energy side of the resonance. However, the effect of the orientation fluctuations on a_2 is large; it causes a considerable attenuation in a_2 in agreement with the experiments.

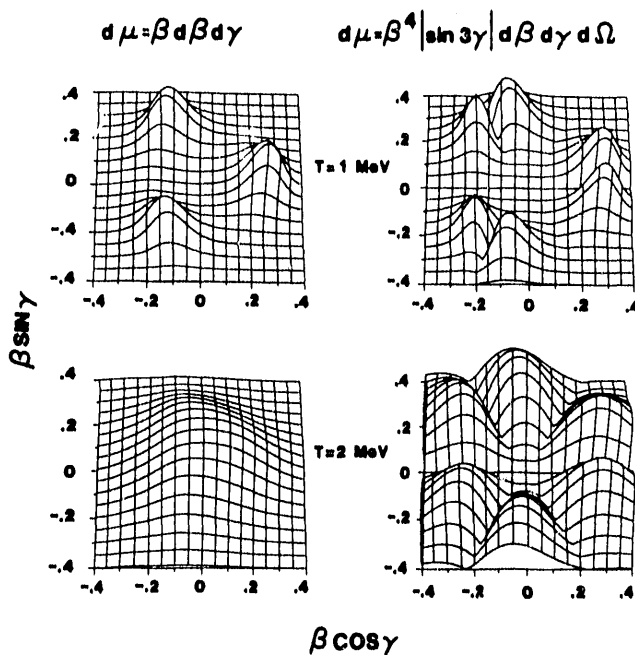
The dotted lines in Fig. 10 show the results of the calculations where the fluctuations are evaluated with a metric used by other authors [28,30,31]

$$D[\alpha] = \beta d\beta d\gamma \quad (5.20)$$

which does not include orientation fluctuations. We see that these results are in strong disagreement with the measured GDR cross-sections. The GDR widths are considerably underestimated by the calculations and their shape is different from the experimental ones. The a_2 's on the other hand are close to those calculated with the metric (4.4) and with orientation fluctuations. If a temperature-dependent width is added to fit the experimental width of the GDR cross-sections, then a disagreement with a_2 will result. Also, if orientation fluctuations are included with the metric (5.22), then a_2 will be strongly attenuated relative to the experiment. Thus only a theory with intrinsic shape and shape orientation fluctuations according to the unitary metric (4.4) can reproduce both the observed cross-sections and a_2 's. The good agreement between experiment and theory is also an indirect confirmation of the existence at finite temperatures of non-collective oblate shapes whose deformation increases with spin.

We have seen that the choice of the metric plays an important role when

Fig. 11. Comparison of the unitary metric (5.4) and the metric $\beta d\beta d\gamma$ (Eq. (5.20)). Probability densities are shown for ^{186}Er at $T=1$ and 2 MeV ($\omega=0$). Left: using the metric (5.20); right: using the unitary metric.



compared with the experimental results. The main difference between the two metrics is that the unitary metric (5.4) favors large and triaxial deformations far more than Eq. (5.20). This is illustrated in Fig. 11 which shows for both metrics the probability density for an intrinsic deformation in cartesian coordinates $\beta \cos \gamma$ and $\beta \sin \gamma$. Notice the peaks along triaxial shapes in the case of the unitary metric. The difference between the two is more noticeable at higher temperatures.

To understand the effect of orientation fluctuations we use the approximation of Section 5.2. Since σ does not depend on orientation they do not affect the average much. However when we average a_2 in Eq. (5.19) over orientation, we obtain (for axial nuclei)

$$a_2 = \frac{f_{\perp} - f_{\parallel}}{2f_{\perp} + f_{\parallel}} r \quad (5.21)$$

where \parallel and \perp denote the direction parallel and perpendicular to the symmetry axis. r is an attenuation factor given by

$$r = \left\langle \frac{3 \cos^2 \theta - 1}{2} \right\rangle = \frac{3}{4x} e^x / \int_0^1 e^{xz^2} dz = \frac{3}{4x} - \frac{1}{2} \quad (5.22)$$

where

$$x = (I_{\parallel} - I_{\perp}) \omega^2 / 2T \quad (5.23)$$

The attenuation factor r is shown vs. x in Fig. 12. Notice that the attenuation is smaller (i.e. r closer to 1) when $|x|$ is larger. From (5.23) this happens when the spin is higher (and there are less fluctuations in orientation) or when $\Delta I = |I_{\parallel} - I_{\perp}|$ is larger (at larger deformation).

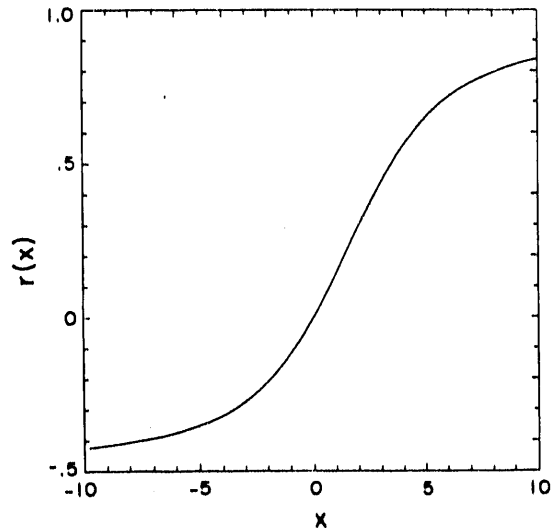


Fig. 12. Attenuation factor r (Eq. (5.22)) vs. x (Eq. (5.23)). For prolate shapes $x < 0$ and for oblate shapes $x > 0$.

The value of a_2 is also sensitive to the intrinsic shape, and its magnitude increases with deformation (for a spherical nucleus $a_2=0$). Intrinsic shape fluctuations tend to drive the most probable deformation to higher values (compared with the equilibrium deformation), for which the resulting anisotropy is larger. For example ^{90}Zr at $T=1.6$ MeV and $J=22 \hbar$ has an equilibrium deformation of $\beta \approx 0.08$ but a most probable $\beta \approx 0.31$. The enhancement of a_2 due to intrinsic shape fluctuations is counteracted by its suppression due to orientation fluctuations. Thus the observed a_2 is an indirect indication of the equilibrium shape. In the experiment of Fig. 10 it was therefore possible to demonstrate liquid-drop-like shape changes from spherical to oblate with increasing spin [33,34].

5.4 Sensitivity of the GDR to Shape

As shown in Section 5.3 our theory provides a good description of the available data. Other examples for the GDR cross-section in the strongly deformed rare-earth region are shown in Fig. 13. From the $T=0$ GDR cross-section of ^{166}Er we have determined $E_p=14.4$ MeV and $\Gamma_0=3.64$ MeV. We have calculated the GDR cross-section for ^{166}Er and ^{160}Er for the temperatures and spins shown in the figure. The solid lines are from the experimental data. Again, when the unitary metric is used (dashed lines) we obtain good

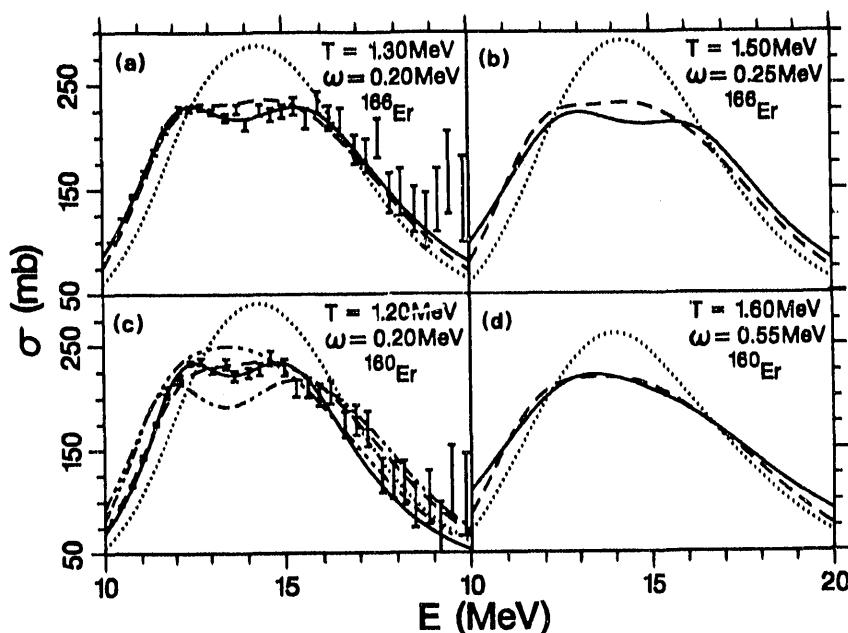


Fig. 13. Comparison of the calculated photoabsorption GDR cross-sections (dashed lines) with the results of CASCADE code fits to the experimental ones (solid lines). (a) ^{166}Er at $T=1.30$ MeV, $\omega=0.20$ MeV (corresponding to an excitation energy $E^*=49.2$ MeV in Ref. 14). (b) ^{166}Er at $T=1.50$ MeV, $\omega=0.25$ MeV ($E^*=61.5$ MeV in Ref. 14). (c) ^{160}Er at $T=1.20$ MeV, $\omega=0.20$ MeV ($E^*=43.2$ MeV in Ref. 14). (d) ^{160}Er at $T=1.60$ MeV, $\omega=0.55$ MeV ($E^*=90.3$ MeV in Ref. 20). The dotted lines represent the calculated GDR with the $\beta\delta\beta dy$ metric. The error bars in (a) and (c) are only suggestive of the accuracy of the experimental measurements and do not represent the actual data.

agreement with the data while for the metric (5.20) (dotted lines) the agreement is poor.

Having established the ability of our theory to provide a quantitative account of the experimental situation, we will now discuss the question of how sensitive the GDR is as a probe of the shape of hot nuclei. Indeed, with increasing T , the thermal fluctuations increase due to two factors: the explicit appearance of T in the denominator of the exponent in (4.2), and the T dependence of the free energy surface. It is the last factor which is associated with the shape changes caused by heating and rotating a deformed nucleus. In order to see the sensitivity of the GDR results to these changes, we show in Fig. 13 (for ^{166}Er at $T=1.2$ MeV and $\omega=0.2$ MeV) the GDR cross-section obtained by using the "wrong" surfaces F in Eq. (4.2): the $T=0$ (the "dot-dot-dashed-dashed" line) and the $T=3$ MeV (the "dot-dot-dot-dashed" line) surfaces. The experimental results clearly indicate that at $T=1.2$ MeV ^{166}Er , though still prolate [14], has a softer energy surface than at $T=0$. However, at higher temperatures ($T \geq 1.6$ MeV) the GDR becomes much less sensitive to variations in the energy surface [32].

In Fig. 14, we have plotted the cross-section's full width at half maximum (FWHM) as contour lines in the $T-\omega$ (or $T-J$) plane for ^{166}Er (a typical deformed nucleus) and for ^{140}Ce (a typical spherical nucleus). The latter nucleus shows a more dramatic change with temperature: its width at $T=2$ MeV is about twice that at $T=0$ MeV (in accord with experiment [18]). This occurs because its free-energy surface "softens" as T rises from 0 to 2 MeV and because as a spherical nucleus it has only a single Lorentzian component at $T=0$. Erbium has a deformed ground state and its FWHM changes more slowly for $T \leq 2$ MeV.

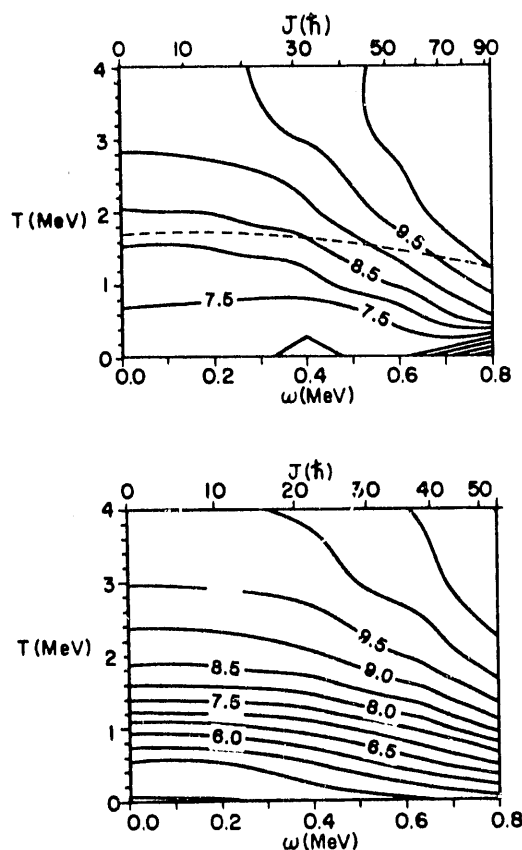


Fig. 14. FWHM contour lines (MeV) in the $T-\omega$ (or $T-J$) plane of the GDR for ^{166}Er (top) and ^{140}Ce (bottom). The shape transition line is shown by the dashed line in the upper figure.

Another interesting phenomenon is that for both nuclei the widths increase much more slowly at temperatures above 3 MeV. This is associated with the disappearance of shell effects in this temperature region.

6. Dissipation and Time-dependent Fluctuations in Hot Nuclei

Though the static fluctuation theory works reasonably well for many of the observed GDR cross-sections, there are several cases, in particular at higher-temperatures ($T \geq 2$ MeV) where the above theory [35] overestimates the observed width of the GDR [20]. It was recently suggested that in analogy with nuclear magnetic resonance in condensed matter systems [54] and with rotational damping of $B(E2)$ transitions in the continuum [37], the GDR could display a phenomenon known as "motional narrowing" [38]. The physical reason for this is that the nucleus is hopping so fast between its various shapes that the GDR does not have enough time to probe separately each nuclear shape. Thus there is less broadening of the GDR due to its coupling with the low-lying quadrupole collective states. This idea was incorporated in Ref. 38 within the framework of a microscopic model for the strength function based on a description of the compound nucleus by random matrix theory. Although the model is successful in explaining motional narrowing, it is rather complicated and very difficult to solve at intermediate situations where the time scale for hopping between shapes is comparable to that associated with the spread of the GDR frequencies from shape fluctuations. Furthermore, this theory is proper for a single resonance and does not take into account the coupling between the various resonances of a deformed nucleus. In particular, when the Gaussian Orthogonal Ensemble (GOE) of random matrices is used and under certain approximations, one always obtains in the adiabatic limit the Wigner semicircular distribution, which is inconsistent with previous adiabatic theories.

We have introduced a relatively simple macroscopic theory of time-dependent fluctuations [35,36], within the framework of the Landau theory, which generalizes our previous theory of fluctuations to non-adiabatic situations for the GDR. The dynamics of the quadrupole shape fluctuations are described by a model analogous to Brownian motion where the quadrupole degrees of freedom play the role of the heavy particle immersed in a fluid and all the other nuclear degrees of freedom play the role of the surrounding fluid molecules. We assume that at the temperatures of interest the quadrupole motion is overdamped. The thermodynamical driving force (to equilibrium) is proportional to the free energy gradient (with respect to $\alpha_{2\mu}$) and the random force describes the interaction of the quadrupole shape parameters $\alpha_{2\mu}$ with all other degrees of freedom. Since the Landau expansion of the free energy contains terms up to fourth order in the deformation, the equation of motion for $\alpha_{2\mu}$ has the form of a non-linear Langevin equation [55]. When compared with the theory of Section 5, the current model contains only one additional parameter; it is proportional to the mean relaxation rate of the quadrupole motion. This parameter spans the full range between the adiabatic limit and the sudden limit in which the time scale for changes in the quadrupole shape is much shorter as compared to the time scale associated with the difference in GDR frequencies over a typical change in deformation. The other parameter in the theory, i.e. the magnitude of the correlation of the random force, is completely determined in terms of the relaxation parameter through the

fluctuation-dissipation theorem. This theorem must be satisfied in order for the equilibrium distribution to be a solution of the equation of motion. Indeed, what we have is a picture of a dynamical equilibrium of the nucleus, in which the shape fluctuates in time but the distribution of shapes at any given moment is the equilibrium distribution.

6.1 Langevin Equation

Assuming the quadrupole vibrations to be overdamped at the temperatures of interest, we model the quadrupole fluctuations by an equation of the Brownian motion type

$$\dot{\alpha}_{2\mu} = -\frac{1}{\chi} \frac{\partial F}{\partial \alpha_{2\mu}^*} + f_{2\mu}(t) \quad (6.1)$$

$F(T, \omega, \alpha_{2\mu})$ is the free energy surface at temperature T and angular velocity ω , so that $-\partial F/\partial \alpha_{2\mu}^*$ plays the role of an external average driving force at finite temperature. The quantity $f_{2\mu}(t)$ is a random force which describes the interaction of the quadrupole shape degrees of freedom with all the others. It is assumed gaussian and stationary, satisfying the relations

$$\begin{aligned} \langle f_{2\mu}(t) \rangle &= 0 \\ \langle f_{2\mu}(t) f_{2\mu'}^*(t') \rangle &= \xi \delta(t-t') \delta_{\mu\mu'} \end{aligned} \quad (6.2)$$

where ξ characterizes the magnitude of the correlation. The correlations in (6.2) express the physical assumption that the forces $f_{2\mu}$ vary rapidly on the time scale of the variation of $\langle \alpha_{2\mu} \rangle$. Notice that, similar to $\alpha_{2\mu}$, $f_{2\mu}$ are complex but satisfy the reality condition

$$f_{2\mu}^*(t) = (-)^{\mu} f_{2-\mu}(t) \quad (6.3)$$

Relations (6.2) imply that the real and imaginary parts of $f_{2\mu}$ are uncorrelated. Taking the average of (6.1) we find

$$\langle \dot{\alpha}_{2\mu} \rangle = -\frac{1}{\chi} \left\langle \frac{\partial F}{\partial \alpha_{2\mu}^*} \right\rangle \quad (6.4)$$

For a quadratic F this describes the relaxation of the average deformation to its equilibrium value defined by $\langle \partial F/\partial \alpha_{2\mu}^* \rangle = 0$. The parameter χ of the model is then proportional to the mean relaxation time of $\alpha_{2\mu}$ to its equilibrium value. The first order equation (6.1) is correct if the quadrupole motion is strongly overdamped. Otherwise we have to use a second-order equation which contains an additional mass parameter. The reduction from the second to first-order equation is discussed elsewhere

[56]. Also $1/\chi$ in Eq. (6.1) and the correlation function (6.2) can be more generally an anisotropic tensor $(1/\chi)_{\mu\mu}$, which depends on $\alpha_{2\mu}$. In this paper we have taken the simplest possible form which is isotropic. If for example the relaxation times for the nuclear orientation are different from those of the intrinsic shape we have to consider an anisotropic $1/\chi$ in (6.1).

Equation (6.1) is a non-linear Langevin equation. The (non-linear) driving force is found by taking the derivatives of the Landau expansion of F analytically in the rotating frame. Notice that it is important to consider this expansion for a general $\alpha_{2\mu}$ and not just for situations in which a principal axis of the nucleus is parallel to $\vec{\omega}$. Indeed, time-dependent fluctuations in the orientation of the nucleus are possible. We find

$$\frac{\partial F}{\partial \alpha_{2\mu}^*} = 2A \alpha_{2\mu} + 3B b_{\mu\nu} \alpha_{2,\mu-\nu} \alpha_{2\nu} + 4C(-)^{\nu} \alpha_{2\nu} \alpha_{2-\nu} \alpha_{2\mu} ,$$

$$- \left[2(I_1+D) \alpha_{2\mu} \delta_{\mu,\pm 2} + (2I_1+D) \alpha_{2\mu} \delta_{\mu,\pm 1} - (R-2I_1 \alpha_{2\mu}) \delta_{\mu,0} \right] \omega^2$$

(6.5)

where $b_{\mu\nu}$ is proportional to a Clebsch-Jordan coefficient, $b_{\mu\nu} = \sqrt{7/2} \langle 2 \mu-\nu \ 2\nu | 2\mu \rangle$. Here $\vec{\omega}$ is chosen parallel to the z-axis in the laboratory frame, and A,B,C,... are the Landau parameters of Section 3.

The Langevin equation (6.1) defines a stochastic Markov process which determines an ensemble of "trajectories" $(\alpha_{2\mu}(t))$. At any time t we can then construct a distribution $P(\alpha_{2\mu}, t)$ of the shapes such that $P(\alpha) \Pi_{\mu} d\alpha_{2\mu}$ is the probability of finding a shape α in the volume element $\Pi_{\mu} d\alpha_{2\mu}$ around $\alpha_{2\mu}$. The equation of motion of P is discussed in the next section.

6.2 Fokker-Planck Equation

Since the process $\alpha_{2\mu}(t)$ in (6.1) is Markovian, it obeys a master equation whose form can be determined from the so-called jump moments. Starting from a given shape $\alpha_{2\mu}$ the average jump (first moment) is calculated from (6.1) to be

$$\langle \Delta \alpha_{2\mu} \rangle = - \frac{1}{\chi} \frac{\partial F}{\partial \alpha_{2\mu}^*} \Delta t$$

(6.6)

while the second moments are

$$\langle \Delta \alpha_{2\mu} \Delta \alpha_{2\mu'} \rangle = \xi \delta_{\mu\mu'} \Delta t$$

(6.7)

The distribution $P(\alpha_{2\mu}, t)$ therefore satisfies a Fokker-Planck equation [57]

$$\frac{\partial P}{\partial t} = - \frac{\partial}{\partial \alpha_{2\mu}} \left[- \frac{1}{\chi} \frac{\partial F}{\partial \alpha_{2\mu}^*} P \right] + \frac{1}{2} \xi \frac{\partial^2 P}{\partial \alpha_{2\mu} \partial \alpha_{2\mu}^*} \quad (6.8)$$

The first term on the right of (6.8) is known as the "drift" term while the second is the "diffusion" term. ξ then has the meaning of the macroscopic diffusion constant and (6.7) is just the Einstein relation which relates ξ to the microscopic jumps of $\alpha_{2\mu}$.

6.3 Fluctuation-Dissipation Theorem

Any solution to the Fokker-Planck equation converges to the stationary solution $P_{st}(\alpha_{2\mu})$ which satisfies

$$\frac{\partial}{\partial \alpha_{2\mu}} \left[\frac{1}{\chi} \frac{\partial F}{\partial \alpha_{2\mu}^*} P_{st} + \frac{1}{2} \xi \frac{\partial P_{st}}{\partial \alpha_{2\mu}^*} \right] = 0 \quad (6.9)$$

A solution to (6.9) is

$$P_{st} \propto e^{-\frac{2}{\chi\xi} F} \quad (6.10)$$

Since (6.10) should coincide with the equilibrium distribution

$$P_{eq} \propto e^{-F/T} \quad (6.11)$$

we conclude that

$$\xi = \frac{2T}{\chi} \quad (6.12)$$

Eq. (6.12) determines the correlation function of the random force in (6.1). Equation (6.12) is just a special case of the fluctuation-dissipation theorem which connects the fluctuations (of the random force) at equilibrium with a dissipation parameter characterizing the relaxation to equilibrium. Relation (6.12) determines ξ in our model (6.1), so that the only undetermined parameter of the model is χ .

In terms of P_{eq} , Eq. (6.1) can be rewritten as

$$\frac{\partial P}{\partial t} = \frac{\partial}{\partial \alpha_{2\mu}} \left[P_{eq} \frac{\partial}{\partial \alpha_{2\mu}^*} \left(\frac{1}{2} \xi \frac{P}{P_{eq}} \right) \right] \quad (6.13)$$

To show that any solution of (6.1) converges to P_{eq} we define the relative information content [58] H of P with respect to P_{eq} by

$$H = \int D[\alpha] P \ln \left(\frac{P}{P_{eq}} \right) \quad (6.14)$$

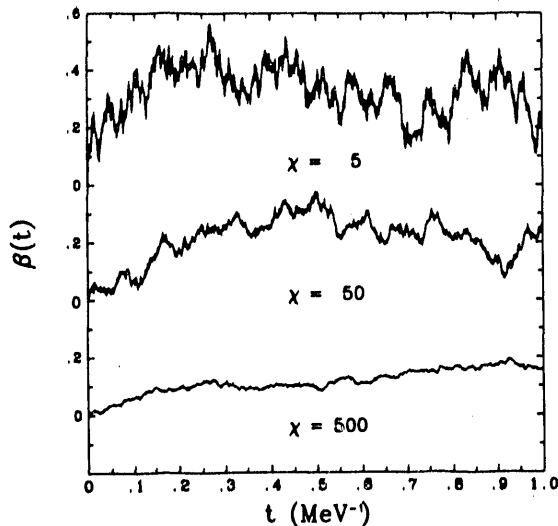
where $D[\alpha] = \prod_{\mu} d\alpha_{2\mu}$. Using (6.13) we find that

$$\frac{dH}{dt} = \int D[\alpha] \frac{\partial P}{\partial t} \ln \left(\frac{P}{P_{eq}} \right) - \frac{1}{2} \xi \int D[\alpha] \frac{P}{P_{eq}} \sum_{\mu} \left| \frac{\partial}{\partial \alpha_{2\mu}} \left(\frac{P}{P_{eq}} \right) \right|^2 \leq 0, \quad (6.15)$$

is always non-positive. Thus H decreases monotonically in time unless $P=P_{eq}$ where $dH/dt=0$. For $P \neq P_{eq}$ we have $dH/dt < 0$ and H will decrease gradually to zero so that any P will eventually decay to P_{eq} (where $H=0$). In fact H is a measure of the entropy difference of the equilibrium distribution relative to the instantaneous distribution P .

If at time $t=0$, $P=P_{eq}$, then initially $H=0$ and therefore $H=0$ for all times t so that $P=P_{eq}$ for any t . This is the stationary solution of the Fokker-Planck equation (6.8). The corresponding ensemble of solutions $\{\alpha_{2\mu}(t)\}$ of the Langevin equation is obtained when the initial shapes $\{\alpha_{2\mu}(0)\}$ are distributed according to P_{eq} . They describe a stationary Markov process. This process describes an equilibrated nucleus at temperature T for which the shape fluctuates in time but which at any given

Fig. 15. Typical shape trajectories β vs. time t for ^{112}Sn at $T=1.8$ MeV and $\omega=0.535$ MeV, obtained from the solution of (6.1). The three trajectories shown correspond to various values of χ : $\chi=500$ (adiabatic limit), $\chi=50$ and $\chi=5$ (sudden limit).



time has the same distribution P_{eq} . In what follows $(\alpha_{2\mu}(t))$ will denote the above process.

In section 6.4 we shall explain how the ensemble $(\alpha_{2\mu}(t))$ can be constructed by Monte-Carlo techniques. In Figure 15 we show three typical "trajectories" $\beta(t)$ obtained in a Monte-Carlo solution of (6.1) for three different values of the parameter χ . Since χ is proportional to the relaxation time of $\beta(t)$, the decay of $\beta(t)$ to its equilibrium value is faster as χ gets smaller. According to (6.12), the variance of the random force, which is proportional to ξ , is inversely proportional to χ . Thus as χ gets smaller the r.m.s. value of the random force gets larger and the motion is less smooth and more erratic when shown on the same time scale.

6.4 Non-Adiabatic Theory of the GDR

The giant dipole resonance absorption cross-section $\sigma(\epsilon)$ and angular anisotropy $a_2(\epsilon)$ can be calculated from the Fourier transform of the temporal autocorrelation functions of the dipole operator \vec{D} at equilibrium (see Eqs. (5.7) and (5.8)). Such a correlation function can be determined from an equation of motion for \vec{D} . In the following we will assume that the giant vibrations are described by a three-dimensional damped harmonic oscillator rotating with angular velocity $\vec{\omega}$. The vibration frequencies and intrinsic damping widths are assumed to depend on the quadrupole deformation as in the adiabatic theory of Section 5. Since the quadrupole deformation is fluctuating in time according to a stochastic process, the dipole equation also describes a stochastic process which is coupled to the Langevin equation.

Here we shall denote by \vec{D} the dipole operator in the frame which is rotating with constant angular velocity $\vec{\omega}$ and by \vec{P} the canonical conjugate momentum. Since the nuclear shape and orientation are fluctuating, this frame is usually not the intrinsic frame of the nucleus. We have

$$\begin{aligned} \dot{\vec{D}} &= \vec{P} - \vec{\omega} \times \vec{D} - \frac{1}{2} \Gamma \vec{D} \\ \dot{\vec{P}} &= -E^2 \vec{D} - \vec{\omega} \times \vec{P} - \frac{1}{2} \Gamma \vec{P} \end{aligned} \quad (6.16)$$

where E and Γ are the frequency and damping matrices, respectively. E is the matrix which in the principal intrinsic frame is diagonal with elements given by Eq. (5.9).

The transformation from the rotating frame to the principal intrinsic frame is the one which diagonalizes $\alpha_{2\mu}$. Thus in the rotating frame

$$E = E_0 \exp \left[- \sqrt{\frac{5}{4\pi}} Q \right] \quad (6.17)$$

where the matrix Q in cartesian coordinates is

$$Q = \begin{pmatrix} -\alpha_{20}/2 + \sqrt{3/2} \operatorname{Re} \alpha_{22} & \sqrt{3/2} \operatorname{Im} \alpha_{22} & -\sqrt{3/2} \operatorname{Re} \alpha_{21} \\ \sqrt{3/2} \operatorname{Im} \alpha_{22} & -\alpha_{20}/2 - \sqrt{3/2} \operatorname{Re} \alpha_{22} & -\sqrt{3/2} \operatorname{Im} \alpha_{21} \\ -\sqrt{3/2} \operatorname{Re} \alpha_{21} & -\sqrt{3/2} \operatorname{Im} \alpha_{21} & \alpha_{20} \end{pmatrix}. \quad (6.18)$$

The damping matrix Γ is then given from the power law (5.17)

$$\Gamma = \Gamma_0 \left(\frac{E}{E_0} \right)^\delta = \Gamma_0 \exp \left[-\delta \sqrt{\frac{5}{4\pi}} Q \right] \quad (6.19)$$

as in the adiabatic case.

The GDR equations of motion (6.16) are coupled to the quadrupole equation (6.1) through the α dependence of E and Γ . They thus also describe a stochastic process. For any given solution $\alpha_{2\mu}(t)$ of (6.1) we can solve (6.16) for $\vec{D}(t)$. The transformation from $\vec{D}(0)$, $\vec{P}(0)$ to $\vec{D}(t)$, $\vec{P}(t)$ (for a given $\alpha_{2\mu}(t)$) is linear so that it is sufficient to solve (6.16) for six possible independent initial conditions for $\vec{D}(0)$ and $\vec{P}(0)$. The correlation function $\langle \vec{D}(t) \vec{D}(0) \rangle$ can then be calculated by averaging over the whole ensemble $\{\alpha_{2\mu}(t)\}$ if the initial dipole correlations (at $t=0$) are known.

In deriving the initial dipole correlation we are guided by the limit where $\alpha_{2\mu}$ are constant (independent of time). In this limit the correlation function (for fixed $\alpha_{2\mu}$) should give the same contribution to the GDR cross-section that we have assumed in the adiabatic fluctuation theory. This initial correlation function is found to be

$$\langle \vec{D}(0) \vec{D}(0) \rangle = \frac{1}{2} E^{-1} \quad (6.20a)$$

which is simply the ground state expectation of \vec{D}^2 . The other relevant initial condition

$$\langle \vec{P}(0) \vec{D}(0) \rangle = -\frac{1}{2} \quad (6.20b)$$

also follows from considering the ground-state giant resonance state vector.

The degree of adiabaticity of the process is determined by the parameter χ . To see that, we define the adiabaticity parameter η as the ratio between the frequency spread ΔE of the GDR due to variations in the static deformation and the mean relaxation rate λ of the quadrupole motion

$$\eta = \frac{\Delta E}{\lambda} \quad (6.21)$$

We can estimate the frequency spread from

$$\Delta E = \sqrt{5/4\pi} E_0 \Delta\beta \quad (6.22)$$

In (6.22), $(\Delta\beta)^2$ is the variance of β at equilibrium. λ in (6.21) is given by $\lambda=1/t_c$, where the relaxation time t_c can be shown to be [36]

$$t_c \approx \chi \frac{\langle \Delta\alpha_{2\mu} \Delta\alpha_{2\mu}^* \rangle}{5T} \quad (6.23)$$

We then find

$$\eta \approx \frac{E_0}{\sqrt{20\pi}} \frac{\chi}{T} (\Delta\beta) \langle \Delta\alpha_{2\mu} \Delta\alpha_{2\mu}^* \rangle \quad (6.24)$$

Thus, η is proportional to the parameter χ of Eq. (6.1). The adiabatic limit corresponds to $\eta \gg 1$ ($\chi \rightarrow \infty$). The opposite limit $\eta \ll 1$ is referred to as the sudden limit, where the quadrupole deformation fluctuates very rapidly. In the adiabatic limit ($\eta \gg 1$) we can assume the quadrupole deformation $\alpha_{2\mu}$ in the GDR equations (6.16) to be frozen at its initial value $\alpha_{2\mu}(0)$, so that the Fourier transform of the dipole correlation function (for a fixed $\alpha_{2\mu}(0)$) is a superposition of Breit-Wigner curves. The actual GDR absorption cross-section becomes then the average over the initial distribution, i.e. the equilibrium distribution

$$\sigma_{\text{abs}}(\epsilon; T, \omega) = \frac{\int D[\alpha] e^{-F/T} \sigma(\epsilon; \alpha_{2\mu})}{\int D[\alpha] e^{-F/T}} \quad (6.25)$$

and $D[\alpha] = \prod_{\mu} d\alpha_{2\mu} = \beta^4 |\sin 3\gamma| d\beta d\gamma d\Omega$. Eq. (6.25) is identical with our previous adiabatic model of Section 5.3. Furthermore, the unitary metric (4.4) emerges as the one which should be used in the adiabatic limit if (6.1) describes the correct dynamical evolution of $\alpha_{2\mu}$.

To solve the stochastic equations (6.1) and (6.16), and to determine the dipole correlation function in the general case, we proceed as follows:
 (i) We choose an initial ensemble of quadrupole deformations $\{\alpha_{2\mu}(0)\}$ which is distributed according to the equilibrium ensemble $\exp(-F/T)$.
 (ii) For each $\alpha_{2\mu}(0)$ we solve (6.1) by Monte-Carlo techniques [36]. We use a second order stochastic Runge-Kutta method such that

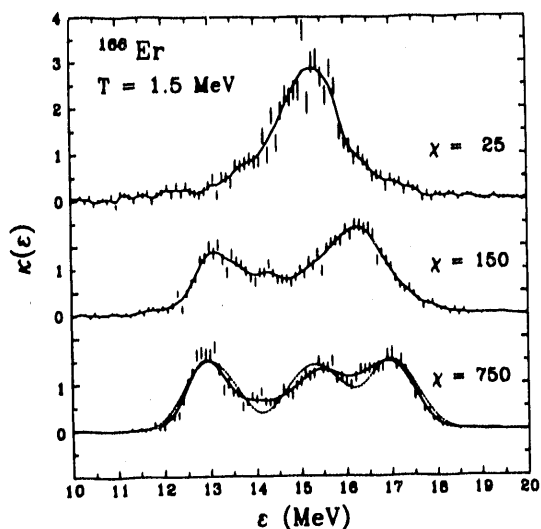
$$\alpha_{2\mu}(t+\Delta t) = \alpha_{2\mu}(t) + g_{2\mu} \Delta t + \sqrt{\Delta t} \xi Y_{2\mu} \quad (6.26)$$

where $g_{2\mu}$ is an average of $-\chi^{-1} \partial F / \partial \alpha_{2\mu}^*$, and the real and imaginary parts of $Y_{2\mu}$ are five independent standard normal random variables. We obtain an ensemble of "shape trajectories" ($\alpha_{2\mu}(t)$) which is equilibrated at any time.

(iii) For each trajectory $\alpha_{2\mu}(t)$ we solve (6.16) for $\bar{D}(t)$ in terms of $\bar{D}(0)$ and $\bar{P}(0)$. The correlation $\langle \bar{D}(t) \bar{D}(0) \rangle$ is then calculated by averaging over the ensemble ($\alpha_{2\mu}(t)$) using the appropriate (quantum mechanical) initial correlation functions (6.20).

Non-adiabatic effects are seen most clearly when one assumes a zero intrinsic width (i.e. $\Gamma_0=0$), so that broadening of the resonance arises only from the coupling to the quadrupole degrees of freedom. We thus consider such a hypothetical ^{166}Er nucleus at $T=1.5$ MeV and $\omega=0$. The solid lines in Fig. 16 are the fit to the Monte Carlo calculations (error bars) of the GDR absorption cross-section and the dotted line is the adiabatic model. At $\chi=750$ we are close to the adiabatic limit where three peaks are seen. At smaller χ the two peaks on the right coalesce and get narrower. Then the left peak starts to move to the right while disappearing and in the sudden limit we have a single narrow Lorentzian. Thus, though the general effect is that of motional narrowing as discussed in Ref. 38, the actual spectral shape of the resonance is also sensitive to η . Note that as the process becomes more sudden it is necessary to take a smaller time step Δt since the quadrupole fluctuations are more erratic.

Fig. 16. The Fourier transforms (solid lines) of the dipole correlation function found from the solution of the stochastic equations (6.1) and (6.16) for various values of χ ($\chi=750, 150,$ and 25). For the purpose of demonstrating the effects of nonadiabaticity we have chosen a hypothetical case where $\Gamma_0=0$ (i.e., no intrinsic damping of the dipole) for ^{166}Er at $T=1.5$ MeV. The bars are the statistical errors associated with the Monte-Carlo calculations and the dashed lines present the adiabatic model of Section 5. Notice that various peaks coalesce and get narrower as the process becomes less adiabatic (χ get smaller).



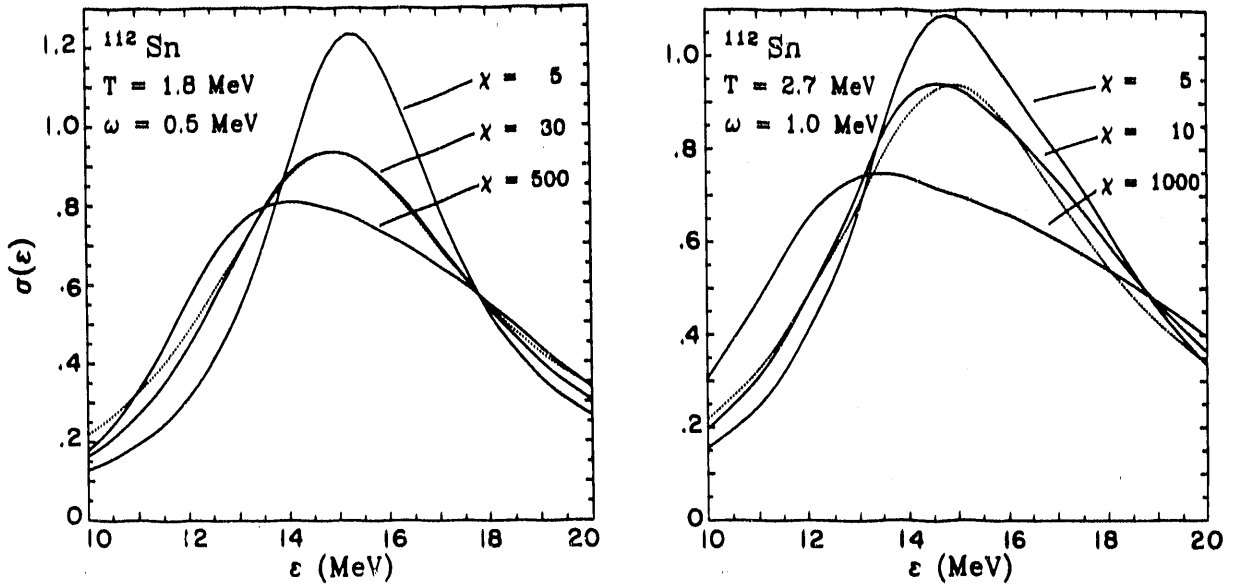


Fig. 17. Comparison with experimental GDR cross-sections for ^{112}Sn [20]. The dotted lines shown are the experimental cross-sections. The solid lines are the results of our stochastic model for several values of χ . The higher and the lower values of χ are the adiabatic and sudden limits, respectively. The intermediate values of χ show the best fit to the data.

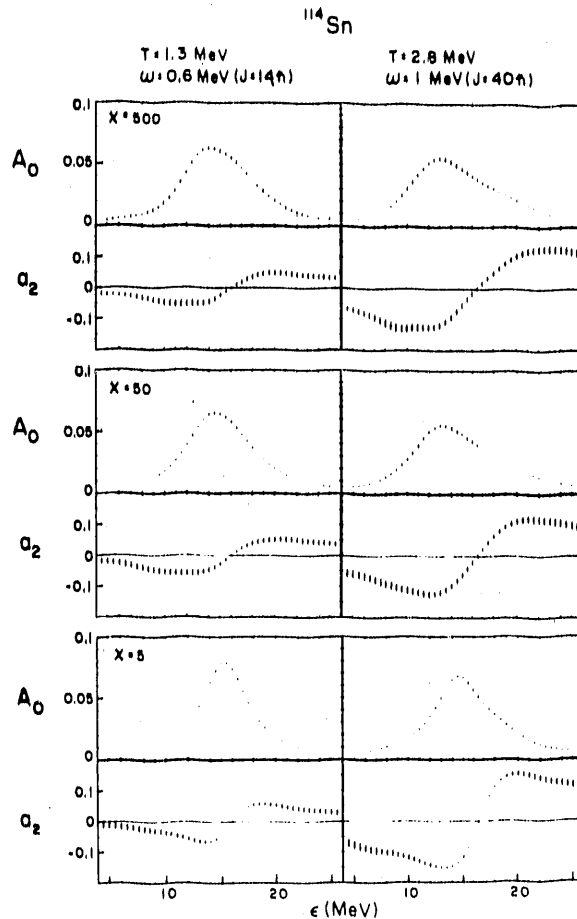
Realistic calculations ($\Gamma_0 \neq 0$) are shown in Fig. 17 for ^{112}Sn where our adiabatic model ($\chi=500$) overestimates the experimental widths [20] (dotted lines). We used $E_0=15.2$ MeV, $\Gamma_0=3.76$ MeV and $\delta=1.6$, and calculated the GDR absorption cross-section for several values of χ . As χ decreases the resonance gets narrower and its structure changes. The values which fit the experiment the closest are shown on the figure and correspond to intermediate η 's.

In the sudden limit $\eta \ll 1$ ($\chi \rightarrow 0$) it is possible to reduce the stochastic equation (6.16) to an equation of motion for $\langle \vec{D} \rangle$ which is basically that of a damped rotating oscillator with some effective frequency and damping width. The effective damping $\tilde{\Gamma}$ is estimated to be (in the $\Gamma_0=0$ case)

$$\tilde{\Gamma} \approx \frac{(\Delta E)^2}{\lambda} = \eta \Delta E \ll \Delta E \quad , \quad (6.27)$$

which is narrower by a factor η from the width in the adiabatic limit. This is exactly the motional narrowing effect discussed in Ref. 38. In realistic calculations Γ_0 has to be added to the r.h.s. of (6.29). The effects of non-adiabaticity on a_2 are shown in Fig. 18 together with those on σ . Two cases are shown for ^{114}Sn , at low ($J=14 \hbar$) and high ($J=40 \hbar$) spins. In the sudden limit the minimum and maximum of $a_2(\epsilon)$ become more sharply peaked and larger in magnitude. They are also closer to the central energy E_0 . These effects are consistent with the motional narrowing in $\sigma(\epsilon)$.

Fig. 18. Non-adiabatic effects on $\sigma \propto A_0$ and a_2 for ^{114}Sn at low spin (left side) and high spin (right side). Both σ and a_2 are shown for various values of χ : $\chi=500$ (adiabatic), 50 and 5 (sudden). Notice the motional narrowing in σ and the stronger peaks in a_2 when the sudden limit is approached.



We have seen earlier that for ^{112}Sn the GDR cross-section is consistent with an intermediate situation between the adiabatic and sudden limit. Thus we expect a_2 to look more like the intermediate cases in Fig. 18. Unfortunately the a_2 's for ^{112}Sn were not measured yet. It will be very interesting to determine them experimentally. This will provide a more crucial test of non-adiabatic effects in the GDR.

7. Quasi-Continuum E2 Transition

At lower excitation energies ($E^* \leq 8$ MeV), the E1 decay rate is lower and E2 transitions above Yrast dominate. The quasicontinuum E2 spectrum has been recently observed [39] by subtracting the discrete lines and the statistical γ -rays, and then decomposing the remaining quasicontinuum into dipole and quadrupole parts. The observed E2 bump is then interpreted as the result of E2 transitions within dense rotational bands in the continuum [39]. These E2 transitions are thus a possible probe of the properties of "warm" nuclei whose excitation energy is below the neutron separation energy. An interesting observation was made through the analysis of the experimental data [39] of warm transitional dysprosium isotopes ($^{152, 154, 156}\text{Dy}$): a strong collective B(E2) of about 300 W.u. was required

to reproduce the measured Doppler shift of the E2 peak as well as the spectral shape.

For transitional nuclei, the shape transition temperature is low [47] ($T_{cr} \sim 0.5 - 1$ MeV). Fig. 19 shows the phase diagram in the energy-spin plane where only the transition lines ($\gamma = -180^\circ$) are displayed. The transitions at $J=0$ happen at $E^* \approx 12, 21$ and 30 MeV for $^{152}, ^{154}, ^{156}$ Dy, respectively. In the experiment of Ref. 39 the γ -cascades start at a given entry point and proceed along different paths determined by the competition between E2 and E1. The most probable path is shown in the above figure by arrows. To estimate $B(E2)$ for a general triaxial rotating shape we assume an asymmetric rotor. If its angular momentum J is large it has in addition to J an approximate good ("wobbling") quantum number n . The E2 transitions proceed along the bands $n = \text{const.}$ with strength [59]

$$B(E2; n, J \rightarrow n, J-2) \approx \frac{5}{16} \pi e^2 Q_{22}^2 \quad (7.1)$$

where Q_{22} is the intrinsic quadrupole moment around the rotation 3 axis. Assuming a uniformly charged ellipsoid we find

$$Q_{22} = \sqrt{\frac{3}{2}} \frac{Z}{5} (R_1^2 - R_2^2) \quad (7.2)$$

where R_1 and R_2 are the semi-axes lengths along the 1 and 2 axes.

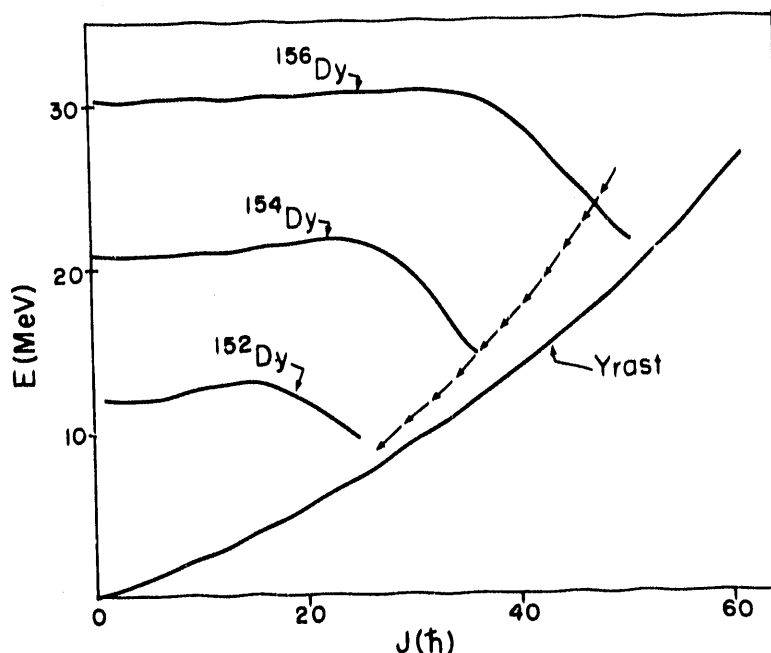


Fig. 19. Phase diagram of $^{152}, ^{154}, ^{156}$ Dy in the energy-spin plane. Shown are the Yrast line and the transition lines. The arrows indicate an approximate most probable γ -ray decay pathway.

If the equilibrium deformation is used in (7.2) we obtain for ^{154}Dy values of $B(E2)$ which vary between 0 (in the non-collective oblate regime) and 180 W.u. along the most probable γ -decay path of Fig. 19. However, if fluctuations in β, γ are taken into account according to the general formula (4.5), we obtained values of 240-300 W.u., in agreement with the experiment. It is interesting to note that the dysposium surfaces may have a local superdeformed minimum. As a result the shape fluctuations are enhanced and lead to the above large values of $B(E2)$.

The fourth order Landau theory of Section 3 does not predict a superdeformed minimum. In order to treat the above transitional nuclei in the Landau framework we have to carry this expansion to sixth order. This is however beyond the scope of the present review.

8. Conclusions

We have reviewed the main ideas and theoretical techniques used in the description of hot nuclei. In the temperature range $1 \leq T \leq 3$ MeV, a macroscopic approach to hot rotating nuclei based on the Landau theory combined with a uniform fluctuation theory in all five quadrupole degrees of freedom can reproduce well measured physical observables. Such observables are the GDR cross-section and angular anisotropy of the emitted γ -rays, and the $B(E2)$ quasi-continuum transitions.

Time-dependent fluctuations play an important role in non-adiabatic situations and comparison with the GDR data can be used to determine a dissipation parameter.

Several interesting theoretical issues are still open:

- (i) In our treatment of fluctuations we have assumed that the shape parameters ($\alpha_{2\mu}$) are classical (for $T \geq 1$ MeV). It is not clear what is the role played by quantal fluctuations. They are certainly important at low temperatures.
- (ii) The role played by higher-order shape multipoles (such as octupole).
- (iii) A theoretical estimate of the damping of quadrupole motion at finite temperature.
- (iv) The importance of temperature fluctuations in the transformation from the canonical to the physical microcanonical ensemble.

On the experimental side it is hoped that with the improvement of the present generation of experiments it will become possible to control more accurately the nuclear phase space variables (temperature and spin). It is also necessary to increase the precision with which quantities such as angular anisotropy are measured.

Acknowledgements

I would like to thank S. Levit, J. Zingman and J. Manoyan for their collaboration on the Landau theory of the nuclear shapes transitions, and B. Bush for his collaboration on shape fluctuations and the GDR in hot nuclei.

DISCLAIMER

This report was prepared as an account of work sponsored by an agency of the United States Government. Neither the United States Government nor any agency thereof, nor any of their employees, makes any warranty, express or implied, or assumes any legal liability or responsibility for the accuracy, completeness, or usefulness of any information, apparatus, product, or process disclosed, or represents that its use would not infringe privately owned rights. Reference herein to any specific commercial product, process, or service by trade name, trademark, manufacturer, or otherwise does not necessarily constitute or imply its endorsement, recommendation, or favoring by the United States Government or any agency thereof. The views and opinions of authors expressed herein do not necessarily state or reflect those of the United States Government or any agency thereof.

References

- [1] B. Borderie et al., Z. Phys. Z316, 243 (1984).
- [2] D. Jacquet et al., Phys. Rev. Lett. 53, 2226 (1984).
- [3] R.J. Charity et al., Phys. Rev. Lett. 56, 13 (1986).
- [4] A.L. Goodman, Nucl. Phys. A352, 30 (1981); K. Tanabe, K. Sugawara-Tanabe and M.J. Mang, Nucl. Phys. A357, 20, 45 (1981); M. Faber, J.L. Egido and P. Ring, Phys. Lett. 127B, 5 (1983); J.L. Egido and P. Ring, Nucl. Phys. A388, 19 (1982).
- [5] L.G. Moretto, Nucl. Phys. A182 (1972) 641.
- [6] M. Brack and P. Quentin, Phys. Lett. 52B, 159 (1974); Phys. Scripta 10A, 163 (1974); P. Quentin and H. Flocard, Ann. Rev. Nucl. Sci 28, 523 (1978).
- [7] A.K. Ignatiuk, I.N. Mikhailov, L.H. Molina, R.G. Nazmitdinov and V. Pomorsky, Nucl. Phys. A346, 191 (1980); J. Diebel, K. Albrecht and R.W. Hasse, Nucl. Phys. A355, 66 (1981).
- [8] P. Bonche, S. Levit and D. Vautherin, Nucl. Phys. A427, 278 (1984); A436, 265 (1985); S. Levit and P. Bonche, Nucl. Phys. A437, 426 (1985).
- [9] J.O. Newton et al., Phys. Rev. Lett. 46, 46 (1981).
- [10] J.J. Gaardhoje, C. Ellegaard, B. Herskind and S.G. Steadman, Phys. Rev. Lett. 53, 148 (1984).
- [11] W. Henneriei et al., Nucl. Phys. A396, 329c (1983).
- [12] B. Haas et al., Phys. Lett 120B, 79 (1983).
- [13] A.M. Sandorfi et al., Phys. Lett. 130B, 19 (1983).
- [14] G.A. Gossett, K.A. Snover, J.A. Behr, G. Feldman and J.L. Osborne, Phys. Rev. Lett. 54, 1456 (1985).
- [15] D. Vautherin and N.V. Vinh Mau, Phys. Lett. 120B, 271 (1983).
- [16] P. Ring, L.M. Robledo, J.L. Egido and M. Faber, Nucl. Phys. A415, 261 (1984).
- [17] H. Sagawa and G.F. Bertsch, Phys. Lett. 146B, 138 (1984); K. Sugawara-Tanabe and K. Tanabe, Phys. Lett. 192B, 268 (1987); Prog. Theor. Phys. 76, 1272 (1986).
- [18] For a review see K.A. Snover, Ann. Rev. Nucl. Part. Sci. 36, 545 (1986).
- [19] J.J. Gaardhoje, C. Ellengaard, B. Herskind, R.M. Diamond, M.A. Deleplanque, G. Dines, A.O. Macchiavelli and F.S. Stephens, Phys. Rev. Lett. 56, 1783 (1986).
- [20] D.R. Chakrabarty, M. Thoennensen, S. Sen, P. Paul, B. Butsch and M.G. Herman, Phys. Rev. C37, 1437, (1988).
- [21] J.J. Gaardhoje, A.M. Bruce and B. Herskind, Nucl. Phys. A482, 121c (1988).
- [22] P. Thirolf, D. Habs, D. Schwalm, R.D. Fisher and V. Metug, Nucl. Phys. A482, 93c (1988).
- [23] K.A. Snover, Nucl. Phys. A482, 13c (1988).
- [24] D.R. Chakrabarty, S. Sen, M. Thoennessen, N. Alamanos, P. Paul, R. Schicker, J. Stachel and J.J. Gaardhoje, Phys. Rev. C36, 1886 (1988).
- [25] Y. Alhassid, S. Levit and J. Zingman, Phys. Rev. Lett. 57, 536 (1986).
- [26] Y. Alhassid, J. Zingman and S. Levit, Nucl. Phys. A469, 205 (1987).
- [27] S. Levit and Y. Alhassid, Nucl. Phys. A413, 439 (1984).
- [28] M. Gallardo, M. Diebel, T. Dossing and R. A. Broglia, Nucl. Phys. A443, 415 (1985).

- [29] Y. Alhassid, B. Bush and S. Levit, Phys. Rev. Lett. 61, 1926 (1988); Nucl. Phys. A482, 57c (1988).
- [30] M. Gallardo, F.J. Luis and R.A. Broglia, Phys. Lett. 191B, 222 (1987); J.M. Pacheco et al., Phys. Rev. Lett. 61, 294 (1988).
- [31] A. Goodman, Phys. Rev. C37, 2162 (1988).
- [32] Y. Alhassid and B. Bush, Nucl. Phys. A509, 461 (1990).
- [33] Y. Alhassid and B. Bush, Phys. Rev. Lett. 65, 2527 (1990).
- [34] J. Gundlach, K.A. Snover, J.A. Behr, C.A. Gossett, M.K.-Habior and K.T. Lesko, Phys. Rev. Lett. 65, 2523 (1990).
- [35] Y. Alhassid and B. Bush, Phys. Rev. Lett. 63, 2452 (1989).
- [36] Y. Alhassid and B. Bush, Nucl. Phys. A514, 434 (1990).
- [37] R. Broglia, T. Dossing, B. Lauritzen and R.B. Mottelson, Phys. Rev. Lett. 53, 326 (1987).
- [38] B. Lauritzen, R.A. Broglia, W.E. Ormand and T. Dossing, Phys. Lett. 207B, 2381 (1988).
- [39] R. Holzmann, T.L. Khoo et al., Phys. Rev. Lett. 62, 520 (1989).
- [40] A. Bohr and B. Mottelson, Nucl. Structure, Vol. 1 (Benjamin, New York, 1969), Ch. 2. App. 2.
- [41] L.D. Landau and E.M. Lifshitz, Statistical Physics, (Pergamon, Oxford, 1950), Part 1, Ch. III.
- [42] A.K. Kerman and S. Levit, Phys. Rev. C24, 1029 (1981).
- [43] Y. Alhassid and J. Zingman, Phys. Rev. C30, 684 (1984).
- [44] B. Lauritzen, P. Arve and G.F. Bertsch, Phys. Rev. Lett. 65, 2835 (1988).
- [45] Ref. 41, Ch. IVX.
- [46] A. Aharony, Multicritical points, in: Critical Phenomena, Lecture Notes in Physics 186 (Springer, New York, 1983) p. 207.
- [47] Y. Alhassid, J. Manoyan and S. Levit, Phys. Rev. Lett. 63, 31 (1989).
- [48] D.L. Hill and J.A. Wheeler, Phys. Rev. 89, 1182 (1953).
- [49] Ref. 41, Ch. XII.
- [50] See in Ref. 40, Vol. 2, Ch. 6.
- [51] J.M. Eisenberg and W. Greiner "Nuclear Theory" (North Holland, Amsterdam, 1975), Vol. 1, Chs. 10-11.
- [52] M. Danos and W. Greiner, Phys. Lett. 8, 113 (1964); M.G. Huber, M. Danos, H.J. Weber and W. Greiner, Phys. Rev. 155, 1073 (1967).
- [53] B. Bush and Y. Alhassid, Yale preprint YCTP-N12-90.
- [54] See, for example, C.P. Slichter, "Principles of Magnetic Resonance," Springer Verlag, New York 1978; P.W. Anderson and P.R. Weiss, Rev. Mod. Phys. 25, 269 (1953); R. Kubo, "Fluctuations Relaxation and Resonance in Magnetic Systems," D. ter Haar ed., Oliver and Boyd, Edinburgh, 1961.
- [55] For a discussion of general non-linear Langevin equations see in R. Balian. Y. Alhassid and H. Reinhardt, Physics Reports 131, 1 (1986).
- [56] Y. Alhassid and B. Bush, Yale preprint YCTP-N11-90.
- [57] See, for example, in N.G. Van Kampen, "Stochastic Processes in Physics and Chemistry" (Amsterdam, North Holland, 1981).
- [58] See for example in "The Maximum Entropy Formalism," ed. R.D. Levine and M. Tribus, (MIT Press, Cambridge, 1978).
- [59] Ref. 40, Vol. 2, Ch. 4.

**DATE
FILMED**

7/17/92

